

# 9 Unconventional Superconductivity: Mechanisms and Experimental Probes

Andreas Kreisel  
Niels Bohr Institute  
Jagtvej 155, 2100 Copenhagen

## Contents

<b>1</b>	<b>Introduction</b>	<b>2</b>
<b>2</b>	<b>Superconducting pairing</b>	<b>2</b>
2.1	Momentum-dependent pairing and anisotropic superconducting order parameter	3
<b>3</b>	<b>Spin fluctuation pairing</b>	<b>10</b>
3.1	Spin susceptibility . . . . .	10
3.2	Pairing interaction . . . . .	11
3.3	Single band model . . . . .	13
3.4	Multiband generalization . . . . .	15
3.5	Sublattice degree of freedom and kagome systems . . . . .	18
<b>4</b>	<b>Spectroscopic probes</b>	<b>22</b>
4.1	Density of states . . . . .	23
4.2	Bound states from impurities . . . . .	24
4.3	Dynamical susceptibility and neutron resonance . . . . .	28
4.4	Spin relaxation rate and Hebel-Slichter peak . . . . .	30

## 1 Introduction

The superconducting state for conventional and unconventional superconductivity exhibits four unusual behaviors which are (i) zero resistance below a characteristic critical temperature  $T_c$  of the material (ii) persistent currents in superconductors of ring shape where currents have been observed to flow for time scales of several years, (iii) perfect diamagnetism as expulsion of a weak magnetic field from the interior of the superconductor and (iv) an energy gap  $|\Delta|$  that opens up in the superconducting state. The last phenomenon is used to characterize the superconducting state in spectroscopic experiments, but has many imprints on thermodynamic and transport properties as at finite temperatures thermal excitations are present. For a full energy gap  $|\Delta|$ , these are an exponentially small number while for superconductors with nodal gaps, the number of excitations exhibit a power law which is inherited to the low temperature specific heat and thermal conductivity as these are governed by the low energy density of states. For conventional superconductors where the superconducting pairing is mediated by electron-phonon interaction, the energy gap turns out to be constant for all momentum states on the Fermi surface of the normal state metal,  $|\Delta_{\mathbf{k}}| = \Delta_0$ . The research field of unconventional superconductivity started with the discovery of superconductivity in the heavy-fermion material  $\text{CeCu}_2\text{Si}_2$  in 1979 [1]. Until then, superconductivity was thought to be restricted to metallic elements and simple compounds and characterized by a superconducting gap  $\Delta_0$  that does not show momentum dependence. Since then many unconventional superconductors were identified experimentally (some example materials are shown in Fig. 1), prominent classes listed according to the time of discovery are (i) heavy-fermion materials where electrons with  $f$ -orbital character are at the Fermi level [1] (ii) 1D organic Bechgaard salts [2], (iii) copper-oxide materials (cuprates) where record high critical temperatures were observed [3] (iv) Fullerenes based on  $\text{C}_{60}$  molecules [4] (v)  $\text{Sr}_2\text{RuO}_4$  as material similar to the cuprates [5] and (vi) iron-based superconductors [6]. Other interesting superconductors where pairing was or is still debated are (a)  $\text{MgB}_2$  with a relatively high  $T_c$  and multiband character [7] (b)  $\text{H}_3\text{S}$  as possible high-temperature superconductor [8] (whereas only under extreme pressure conditions) and (c) Kagome superconductors for example the materials  $A\text{V}_3\text{Sb}_5$   $A=\text{K, Rb, Cs}$  [9].

## 2 Superconducting pairing

The starting point of the theoretical analysis of superconducting pairing in BCS theory is usually the presence of a metallic normal state described by a Fermi sea and the assumption of an attractive interaction of strength  $g_0$  in a shell around the Fermi level of  $\omega_D$ . From this, one can show that there exists a bound state irrespective of the value of  $g_0$  (Cooper problem) or the Fermi sea has an instability towards a superconducting state (BCS theory). The assumption however does not consider the Coulomb interaction between the electrons which is repulsive in nature. Here, we will sketch two mechanisms to still overcome the Coulomb interaction and discuss consequences of this for the order parameter characterizing the superconducting phase. The two possible mechanisms can be summarized by the picture that the electrons avoid each

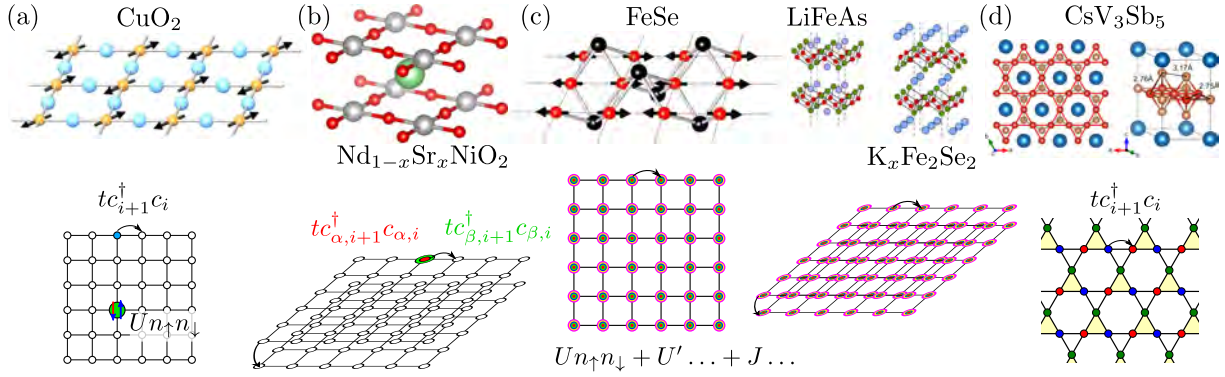


**Fig. 1:** Examples of (potentially) unconventional superconductors: Crystal structure and sketch of models of the electronic structure. (a) Cuprates are often discussed by using a single band Hubbard model on a square lattice [10]. (b) The nickelates might need a multiple orbitals (red/green dot) and three dimensional electronic structure [11]. (c) Fe-based superconductors where all 5 d-orbitals are close to the Fermi level (colored dots) and dispersion in the third direction might play a role (especially for the 122 systems) [10, 12]. Interactions can be parametrized by the parameters  $U$ ,  $U'$  and  $J$ . (d) Kagome superconductors require at least a three band model due to the three different sublattices (red/green/blue) in the unit cell [9].

other in (i) time (retardation) for a conventional pairing mechanism and (ii) in space (momentum-dependent pairing) for unconventional pairing. The first case is realized from the conventional electron-phonon interaction where in a simple picture, one (negatively charged) electron moving through the lattice of atomic cores deforms the lattice. Since the atomic cores are much heavier than the electron, this deformation happens retarded such that a second electron will effectively feel a positive charge that is left “behind” by the first moving electron and therefore yields an effective attractive interaction, see Fig. 2. A detailed analysis of the (dynamic) order parameter  $\Delta(\omega)$  yields that it acquires a sign change in energy in this case. We are not further discussing this mechanism in this lecture and refer to textbooks on this topic [13, 12].

## 2.1 Momentum-dependent pairing and anisotropic superconducting order parameter

The electrons can also overcome the Coulomb interaction by another mechanism which we now illustrate by starting from a Hamiltonian of an electron gas together with a momentum-dependent interaction described by  $V(\mathbf{k}, \mathbf{k}')$ ; its origin will be discussed later. The Hamiltonian is given by

$$H = \sum_{\mathbf{k}, \sigma} \varepsilon_{\mathbf{k}} c_{\mathbf{k}'\uparrow}^\dagger c_{\mathbf{k}\downarrow} + \frac{1}{2N} \sum_{\mathbf{k}, \mathbf{k}'} (V(\mathbf{k}, \mathbf{k}') c_{\mathbf{k}'\uparrow}^\dagger c_{-\mathbf{k}'\downarrow}^\dagger c_{-\mathbf{k}\downarrow} c_{\mathbf{k}\uparrow} + \text{H.c.}), \quad (1)$$

where  $\varepsilon_{\mathbf{k}}$  is the energy dispersion and  $c_{\mathbf{k}\sigma}^\dagger$ ,  $c_{\mathbf{k}\sigma}$  are fermionic creation/annihilation operators of electrons at momentum  $\mathbf{k}$  and spin  $\sigma$ .

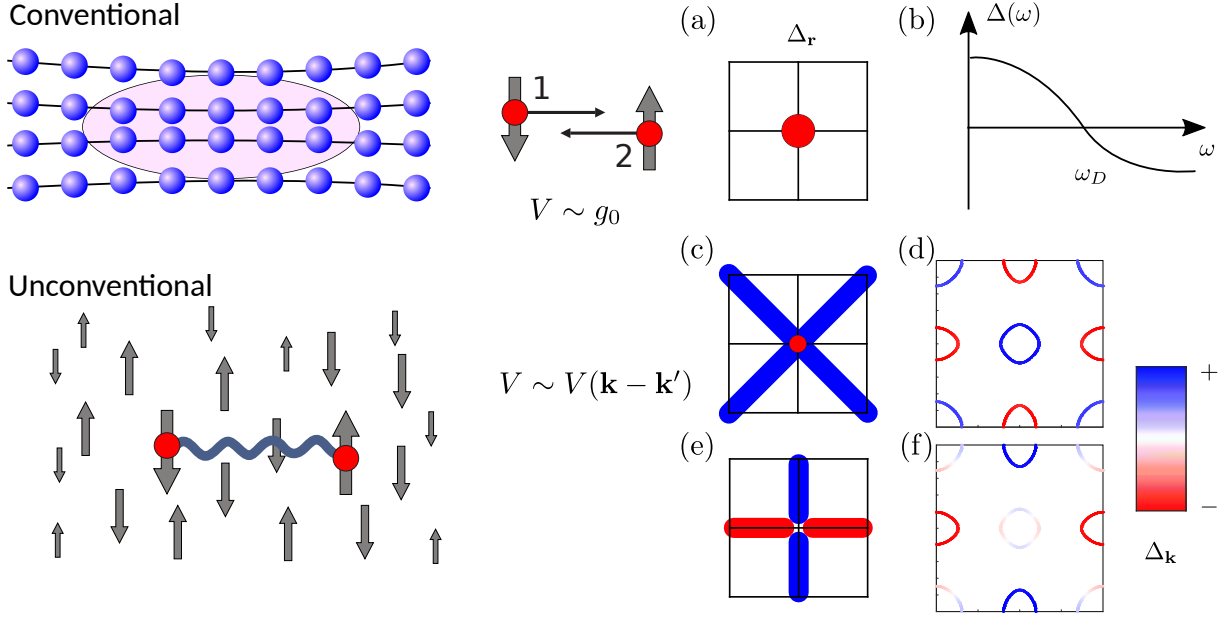


**Fig. 2:** *Conventional pairing:* Two electrons (red dots) attract each other when the first deforms the lattice of positively charged atomic cores (light red region) the second is attracted to that region. The order parameter  $\Delta_{\mathbf{r}}$  is just onsite  $\mathbf{r} = 0$  (a). For the retarded interaction, it changes sign in frequency at the characteristic frequency of the attractive interaction  $\omega_D$  (b) [10, 13]. *Unconventional pairing:* Electrons interact effectively with each other by polarizing the other conduction electrons by the Coulomb interaction. For the antiferromagnetic polarization (“neighbored“ electrons tend to have the opposite spin direction), the second electron can lower its energy in the polarized region of the first electron, leading to an effective interaction (wiggly line) [12, 10] which is momentum dependent. Multiple order parameters can be realized; here two examples are shown: The  $s_{\pm}$  state has the full symmetry of the lattice (c), but exhibits pairing to the next nearest neighbors. A sign change of the order parameter  $\Delta_{\mathbf{k}}$  on the Fermi surface occurs (d). The  $d_{x^2-y^2}$  order parameter has lower symmetry than the lattice since the horizontal bond orders have opposite sign from the vertical ones (e). Similar reduced symmetry of the order parameter in momentum space is given, where the order parameter has symmetry enforced nodes on the Fermi surface and very small gap on the  $\Gamma$  and  $M$  pockets (f) [14].

**Single band model on the square lattice** In view of an example, we are later considering the single band model with nearest neighbor hopping  $t$  and next nearest neighbor hopping  $t'$ ,

$$\varepsilon_{\mathbf{k}} = -2t(\cos k_x + \cos k_y) - 4t' \cos k_x \cos k_y - \mu, \quad (2)$$

where we set the lattice constant  $a = 1$  in the following and use  $t = 1$  as energy unit. This simple model is flexible enough to discuss a number of Fermi surface topologies and stabilize a number different symmetries of the superconducting order parameter. In Fig. 3, we show the band structure and the density of states for variations of  $t' < 0$ . It turns out that one can tune several Lifshitz transitions which are marked as red, blue and green line in the phase diagram in Fig. 4 (left panel) to yield four representative Fermi surface topologies: (1) at large  $|t'|$  the model exhibits electronlike pockets at the X and Y point. Crossing the blue line, these pockets touch and eventually lead to (2) a Fermi surface with electronlike and holelike Fermi pockets.

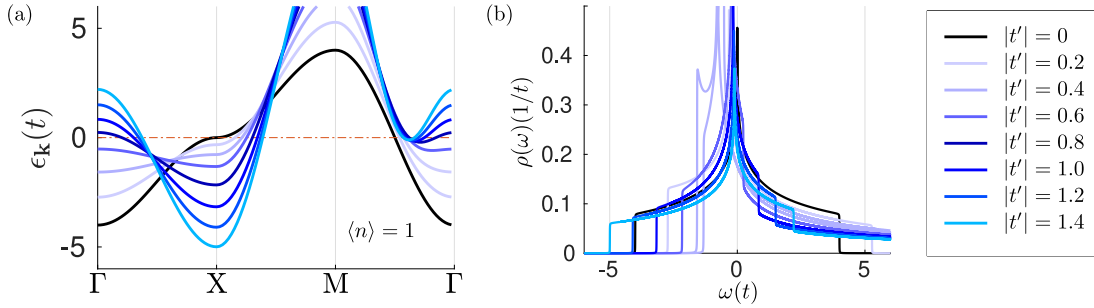


**Fig. 3:** Single band model (a) dispersion along high symmetry path for different choices of  $t' < 0$ , but the chemical potential tuned to stay at half filling  $\langle n \rangle = 1$ . (b) Corresponding density of states  $\rho(\omega)$  exhibiting van Hove singularities from band maxima/minima and saddle points.

Reducing  $|t'|$ , the  $\Gamma$  pocket disappears and a Fermi surface reminiscent for cuprate materials is realized. Crossing the red line of a van Hove singularity with diverging density of states, one reaches (4) a single electronlike pocket around the  $\Gamma$  point, see Fig. 4.

**Mean-field theory** To map the Hamiltonian in Eq. (1) onto a formally non-interacting problem, we use the mean-field approximation. Starting from an interacting Hamiltonian  $H = AB$  containing the product of two operators  $A$  and  $B$  we rewrite the operators as their mean value and a deviation from it,  $A = \langle A \rangle + \delta A$ ,  $B = \langle B \rangle + \delta B$  and ignore the term  $\delta A \delta B$  of second order in the deviations from the mean such that we can replace  $H \rightarrow H_{MF} = \langle A \rangle B + A \langle B \rangle - \langle A \rangle \langle B \rangle$ . This amounts to rewriting the Hamiltonian in a simpler form that can be solved exactly, but depends on the mean values of the two operators as parameters. Next, we need to find a self-consistent solution in which the mean values  $\langle A \rangle$  and  $\langle B \rangle$  are calculated using the eigenvalues and eigenstates of  $H_{MF}$ .

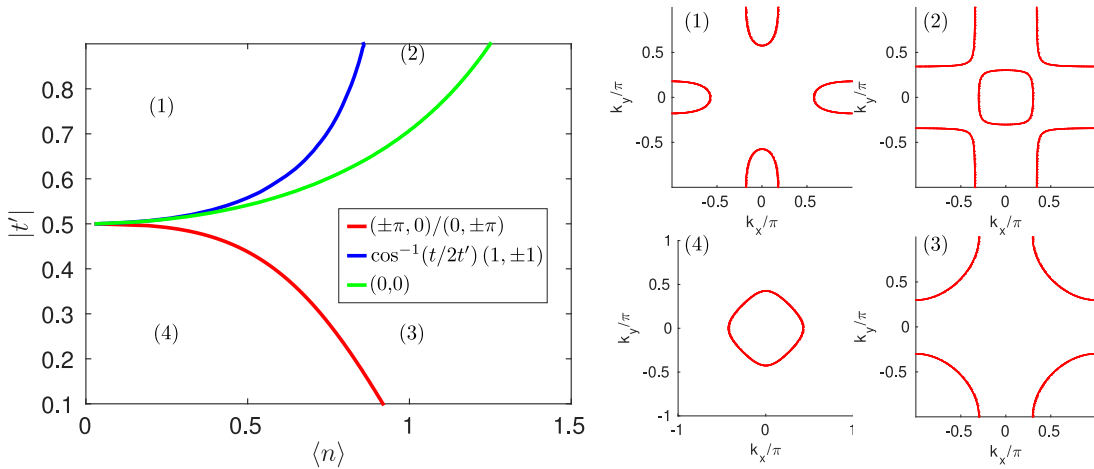


**Fig. 4:** Single band model and Lifshitz transitions: Lines indicate where a point with vanishing Fermi velocity crosses the Fermi level. green: a local band maximum crosses at the  $\Gamma$  point, removing a hole pocket. red: A saddle point crosses and turns electronlike sheets into holelike sheets. blue: Touching of pockets at the zone diagonals. In total four different Fermi surface topologies are possible (1)–(4).

**BCS theory** With the choice of  $A = c_{\mathbf{k}'\uparrow}^\dagger c_{-\mathbf{k}'\downarrow}^\dagger$  and  $B = c_{-\mathbf{k}\downarrow} c_{\mathbf{k}\uparrow}$ , we obtain the mean-field Hamiltonian

$$H_{MF} = \sum_{\mathbf{k},\sigma} \varepsilon_{\mathbf{k}} c_{\mathbf{k}\sigma}^\dagger c_{\mathbf{k}\sigma} + \frac{1}{N} \sum_{\mathbf{k},\mathbf{k}'} V(\mathbf{k},\mathbf{k}') \left( \langle c_{\mathbf{k}'\uparrow}^\dagger c_{-\mathbf{k}'\downarrow}^\dagger \rangle c_{-\mathbf{k}\downarrow} c_{\mathbf{k}\uparrow} + c_{\mathbf{k}'\uparrow}^\dagger c_{-\mathbf{k}'\downarrow}^\dagger \langle c_{-\mathbf{k}\downarrow} c_{\mathbf{k}\uparrow} \rangle - \langle c_{\mathbf{k}'\uparrow}^\dagger c_{-\mathbf{k}'\downarrow}^\dagger \rangle \langle c_{-\mathbf{k}\downarrow} c_{\mathbf{k}\uparrow} \rangle + \text{H.c.} \right). \quad (3)$$

Note that the expectation values  $\langle A \rangle = \langle c_{\mathbf{k}'\uparrow}^\dagger c_{-\mathbf{k}'\downarrow}^\dagger \rangle$  and  $\langle B \rangle = \langle c_{-\mathbf{k}\downarrow} c_{\mathbf{k}\uparrow} \rangle$  are neither singlet nor triplet order parameters at this point. Defining the mean-fields in the singlet ( $s$ ) and triplet ( $t$ ) channel,

$$\Delta_{\mathbf{k}}^{s/t} = -\frac{1}{N} \sum_{\mathbf{k}'} V^{s/t}(\mathbf{k},\mathbf{k}') \langle c_{\mathbf{k}'\uparrow}^\dagger c_{-\mathbf{k}'\downarrow}^\dagger \rangle, \quad (4)$$

where we also have projected to the symmetric (singlet) and antisymmetric (triplet) interactions

$$V^{s/t}(\mathbf{k},\mathbf{k}') = \frac{1}{2} (V(\mathbf{k},\mathbf{k}') \pm V(-\mathbf{k},\mathbf{k}')), \quad (5)$$

we can rewrite the Hamiltonian as

$$H_{MF} = \sum_{\mathbf{k},\sigma} \varepsilon_{\mathbf{k}} c_{\mathbf{k}\sigma}^\dagger c_{\mathbf{k}\sigma} - \sum_{\mathbf{k}} \Delta_{\mathbf{k}}^{s/t*} c_{-\mathbf{k}\downarrow} c_{\mathbf{k}\uparrow} \mp \sum_{\mathbf{k}} \Delta_{\mathbf{k}}^{s/t} c_{\mathbf{k}\uparrow}^\dagger c_{-\mathbf{k}\downarrow}^\dagger + \text{const.} \quad (6)$$

For the mean-field Hamiltonian to obey the Pauli principle, the order parameter has to be even parity in the momentum  $\mathbf{k}$  for the upper sign of  $\mp$ , i.e., the singlet order parameter ( $\Delta_{\mathbf{k}}^s = \Delta_{-\mathbf{k}}^s$ ) and odd parity in the momentum  $\mathbf{k}$  for the lower sign for the triplet order parameter ( $\Delta_{\mathbf{k}}^t = -\Delta_{-\mathbf{k}}^t$ ). Note that one can also assign two spin indices to the order parameter (and consider other quantum numbers such as orbitals or sublattice degrees of freedom). In this case, the order parameter has to be overall odd if all quantum numbers are exchanged. Since our interaction was spin-independent, we can use another spin-quantization axis in the original Hamiltonian and transform the triplet order parameter  $\Delta_{\mathbf{k}}^t = \Delta_{\mathbf{k}\uparrow\downarrow} + \Delta_{\mathbf{k}\downarrow\uparrow}$  into triplet order parameters that formally are in the  $\uparrow\uparrow$  and  $\downarrow\downarrow$  channel while the singlet order parameter remains invariant under such a basis transformation. More generally, the superconducting order parameter matrix can be described by a singlet term and a  $\vec{d}$  vector to parametrize the three components of the triplet order parameter [15].

The mean-field Hamiltonian (with either  $\Delta_{\mathbf{k}}^s$  or  $\Delta_{\mathbf{k}}^t$ ) is now quadratic in the fermionic operators, i.e., describes a non-interacting system and can be diagonalized by a Bogoliubov transformation

$$\begin{pmatrix} \gamma_{\mathbf{k}\uparrow} \\ \gamma_{-\mathbf{k}\downarrow}^\dagger \end{pmatrix} = \begin{pmatrix} u_{\mathbf{k}}^* & -v_{\mathbf{k}} \\ v_{\mathbf{k}}^* & u_{\mathbf{k}} \end{pmatrix} \begin{pmatrix} c_{\mathbf{k}\uparrow} \\ c_{-\mathbf{k}\downarrow}^\dagger \end{pmatrix} \quad (7)$$

which defines new quasiparticle operators  $\gamma_{\mathbf{k}\uparrow}$  that are linear combinations of electron creation and annihilation operators. For this transformation to preserve the anticommutation relations  $\{\gamma_{\mathbf{k}\sigma}, \gamma_{\mathbf{k}'\sigma'}^\dagger\} = \delta_{\mathbf{k},\mathbf{k}'} \delta_{\sigma,\sigma'}$ , we require  $|u_{\mathbf{k}}|^2 + |v_{\mathbf{k}}|^2 = 1$  and can finally fix the value of the coefficients by first inverting the transformation and inserting it into the mean-field Hamiltonian

and then requiring that the terms containing only quasiparticle annihilation operator to vanish. Dropping again constant terms, we can rewrite the Hamiltonian as

$$H_{BCS} = \sum_{\mathbf{k}\sigma} E_{\mathbf{k}} \gamma_{\mathbf{k}\sigma}^\dagger \gamma_{\mathbf{k}\sigma} \quad (8)$$

with the quasiparticle dispersion

$$E_{\mathbf{k}} = \sqrt{\varepsilon_{\mathbf{k}}^2 + |\Delta_{\mathbf{k}}^{s/t}|^2}. \quad (9)$$

Having the quasiparticle dispersion and the transformation at hand, we can evaluate the expectation value in Eq. (4) to obtain the self-consistency condition

$$\Delta_{\mathbf{k}}^{s/t} = -\frac{1}{N} \sum_{\mathbf{k}'} V^{s/t}(\mathbf{k}, \mathbf{k}') \frac{\Delta_{\mathbf{k}'}^{s/t}}{2E_{\mathbf{k}'}} \tanh\left(\frac{\beta E_{\mathbf{k}'}}{2}\right), \quad (10)$$

evaluated at finite temperature. As a side remark, we note that this value of the order parameter indeed minimizes the free energy  $F$ , i.e., the equation above can also be derived from finding a stationary point via  $\frac{\delta F}{\delta \Delta_{\mathbf{k}}} = 0$  [13]. In this case, also the constant terms need to be kept in the Hamiltonian and one sees that the superconducting state indeed has a lower energy than the state of a normal metal once the temperature is low enough that Eq. (10) has a nontrivial solution.

**Linearized gap equation** For a practical discussion of superconducting instabilities given a pairing interaction  $V^{s/t}(\mathbf{k}, \mathbf{k}')$ , it is convenient to linearize this equation by setting  $E_{\mathbf{k}'} = \varepsilon_{\mathbf{k}'}$  on the r.h.s. Observing that the energy gain in the limit of  $\Delta_{\mathbf{k}} \rightarrow 0$ , i.e., at  $T \rightarrow T_c$  has only contributions from states at the Fermi level, the integral over the Brillouin zone becomes a Fermi surface average in the linearized gap equation

$$-\frac{1}{V_G} \int_{FS} dS' V^{s/t}(\mathbf{k}, \mathbf{k}') \frac{g_i(\mathbf{k}')}{|v_F(\mathbf{k}')|} = \lambda_i g_i(\mathbf{k}'). \quad (11)$$

Here  $V_G$  is the volume of the Brillouin zone, the integral  $\int_{FS} dS'$  is over the Fermi surface evaluated at the points  $\mathbf{k}'$ ,  $g_i(\mathbf{k})$  is the gap symmetry function which contains the momentum dependence of the superconducting instability with eigenvalue  $\lambda_i$  where the instability with largest eigenvalue is realized at  $T_c$ . Formally, one can calculate the critical temperature from the eigenvalue by  $T_c = \omega_0 e^{-1/\lambda_i}$ , but the energy scale  $\omega_0$  from the effective pairing interaction is usually not known. In practice the linearized gap equation is solved by discretizing the Fermi surface into a set of Fermi points  $\mathbf{k}'$  with associated area  $l_{\mathbf{k}'}$  and finding the eigenvalues and eigenvectors of the matrix

$$M_{\mathbf{k}, \mathbf{k}'}^{s/t} = -\frac{1}{V_G} \frac{l_{\mathbf{k}'}}{|v_F(\mathbf{k}')|} V^{s/t}(\mathbf{k}, \mathbf{k}'). \quad (12)$$

We note that this matrix is not symmetric since on the r.h.s. the weight  $l_{\mathbf{k}'}/|v_F(\mathbf{k}')|$  appears only in  $\mathbf{k}'$  and not in  $\mathbf{k}$ , but the problem can be cast into the problem of diagonalizing a symmetric

real-valued matrix that guarantees real eigenvalues and eigenvectors as follows: We define a matrix with diagonal elements of the weights  $\Lambda_{\mathbf{k}} = \text{diag}(l_{\mathbf{k}'}/|v_F(\mathbf{k}')|)/V_G$  such that one can trivially obtain  $\sqrt{\Lambda}$  and  $\sqrt{\Lambda}^{-1}$  as diagonal matrices as well. Dropping the  $s/t$  label and the labels  $\mathbf{k}$  and  $\mathbf{k}'$ , one can write Eq. (12) as matrix multiplication,  $M = V\Lambda_{\mathbf{k}'}$ . We multiply this equation with  $\sqrt{\Lambda_{\mathbf{k}}}$  and  $\sqrt{\Lambda_{\mathbf{k}'}}^{-1}$  from left and right to obtain  $\sqrt{\Lambda_{\mathbf{k}}}M\sqrt{\Lambda_{\mathbf{k}'}}^{-1} = \sqrt{\Lambda_{\mathbf{k}}}V\sqrt{\Lambda_{\mathbf{k}'}} \equiv \tilde{M}$ , i.e., a symmetric (real-valued) matrix  $\tilde{M}$ . This matrix now has real eigenvalues  $\lambda_i$  and eigenvectors  $\tilde{g}_i$  obeying  $\tilde{M}\tilde{g}_i = \lambda_i\tilde{g}_i$ . Substituting back the definition of  $\tilde{M}$  and multiplication with  $\sqrt{\Lambda_{\mathbf{k}}}^{-1}$  yields  $M\sqrt{\Lambda_{\mathbf{k}'}}^{-1}\tilde{g}_i = \lambda_i\sqrt{\Lambda_{\mathbf{k}'}}^{-1}\tilde{g}_i$ , in other words  $g_i \equiv \sqrt{\Lambda_{\mathbf{k}'}}^{-1}\tilde{g}_i$  is eigenvector to the original matrix in Eq. (12) to the eigenvalue  $\lambda_i$ .

To evaluate whether the self-consistency equation and/or the linearized gap equation has a non-trivial solution and understand the momentum-dependence of the solution, we now discuss a number of special cases. First, we note that for an attractive interaction (within some energy range  $\omega_D$ ) as obtained from the electron-phonon interaction, it is clear that the minus sign is cancelled by  $V(\mathbf{k}, \mathbf{k}') = g_0$  with  $g_0 < 0$  and we can infer that there exists a solution of the type  $\Delta_{\mathbf{k}}^s = \Delta_0$  because the order parameter can be factored out of the momentum sum and divided out. Transforming now the integral into an energy integral by introduction of the density of states  $\rho(\omega) = \frac{1}{N} \sum_{\mathbf{k}} \delta(\varepsilon_{\mathbf{k}} - \omega)$ , we find the self-consistency equation

$$1 = g_0 \int_{-\omega_D}^{\omega_D} d\omega \rho(\omega) \frac{\tanh\left(\frac{\beta}{2}\sqrt{\omega^2 + |\Delta_0|^2}\right)}{2\sqrt{\omega^2 + |\Delta_0|^2}} \quad (13)$$

leading to the known mean-field temperature dependence of the order parameter that can simply be calculated by a root-finding if the density of states is assumed to be constant close to the Fermi level  $\rho(\omega) \approx \rho(0)$ , see Fig. 5(a).

A calculation of the order parameter at zero temperature in the weak coupling limit yields  $\Delta_0(T=0) = 2\omega_D \exp(-1/(g_0\rho(0)))$  and the critical temperature can be obtained from solving the linearized gap equation by an energy integral. The result  $k_B T_c = \frac{2e\gamma}{\pi}\omega_0 \exp(-1/(g_0\rho(0)))$  is expressed with the Euler constant  $\gamma$ . The universal ratio between critical temperature and order parameter is given by  $2\Delta_0(T=0)/k_B T_c = 2\pi/e\gamma \approx 3.53$ . Experimental deviations from this ratio are sometimes associated with the superconductor being in the strong coupling regime although unconventional pairing, i.e., sign-changing order parameter or anisotropic order parameter can give rise to modifications even in weak coupling BCS theory [16].

**Momentum dependent pairing** For momentum-dependent interactions, we want to give two perspectives. In the first perspective, we expand the interaction  $V^{s/t}(\mathbf{k}, \mathbf{k}')$  close to the Fermi surface in lattice harmonics which are a set of orthogonal functions in the Brillouin zone (similar to the spherical harmonics to expand a function on a sphere). Because of orthogonality and the parity constraints of the order parameter, the dependence on  $\mathbf{k}$  and  $\mathbf{k}'$  can be expanded separately and factorized. For illustration, let us take the pairing interaction

$$V(\mathbf{k}, \mathbf{k}') = U - \frac{3J}{2} (\cos(k_x - k'_x) + \cos(k_y - k'_y)) \quad (14)$$

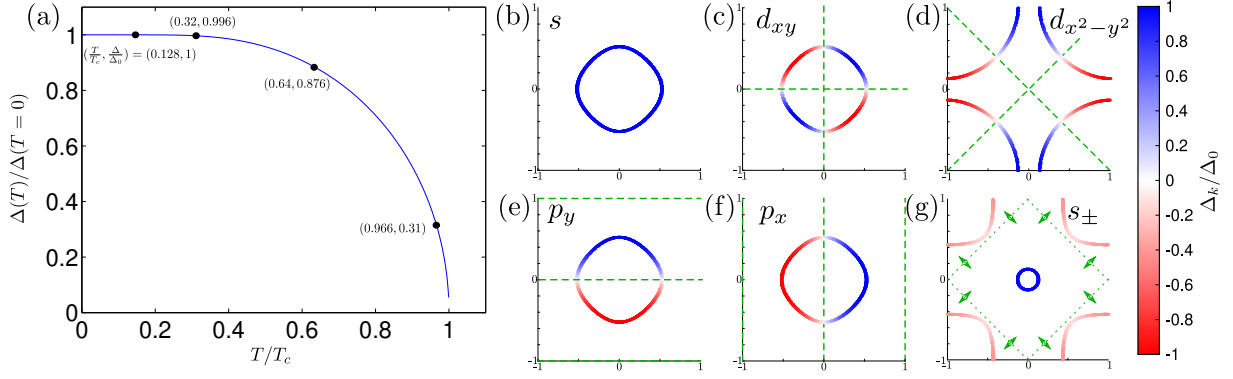


**Fig. 5:** (a) Temperature dependence of the order parameter from self-consistency equation Eq. (13). (b)–(g) Examples of order parameters on a Fermi surface with only electron pocket ( $t'=0$ ,  $n=0.25$  (b), (c), (e), (f)) and ( $t'=-0.35$ ,  $n=0.85$  (d)), ( $t'=-1.2$ ,  $n=0.75$  (g)). Symmetry enforced nodal lines are marked by green dashed lines, accidental nodal lines in panel (g) are marked with dotted lines and can move according to the arrows. Red/blue: sign of order parameter see colorbar.

as it can be derived from rewriting the Hubbard model with nearest neighbor Heisenberg Hamiltonian  $H_{\text{int}} = J \sum_{\langle i,j \rangle} \vec{S}_i \cdot \vec{S}_j$  in the form of Eq. (1) [13]. The singlet interaction is then obtained from the symmetrization, Eq. (5),  $V^s(\mathbf{k}, \mathbf{k}') = U - (3J/2)(\cos k_x \cos k'_x + \cos k_y \cos k'_y)$  which we can rewrite as  $V^s(\mathbf{k}, \mathbf{k}') = V_s + V_d$  with the  $s$ -wave term consisting in a repulsive part and the extended  $s$ -wave interaction  $V_s = U - (3J/4)(\cos k_x + \cos k_y)(\cos k'_x + \cos k'_y)$  and the  $d$ -wave interaction  $V_d = -(3J/4)(\cos k_x - \cos k_y)(\cos k'_x - \cos k'_y)$ . These interactions are now written as products of the lowest harmonics for the respective order parameters, i.e., a constant for a  $s$ -wave order parameter, the function  $f_s(\mathbf{k}) = \cos k_x + \cos k_y$  that is invariant under  $C_4$  rotations of the momentum and the function  $f_d(\mathbf{k}) = \cos k_x - \cos k_y$  that changes sign under a  $C_4$  rotation. When doing a mean-field decoupling in the two channels, i.e., by choosing  $A = f_{s/d}(\mathbf{k}') c_{\mathbf{k}'\uparrow}^\dagger c_{-\mathbf{k}'\downarrow}^\dagger$  and  $B = f_{s/d}(\mathbf{k}) c_{-\mathbf{k}\downarrow} c_{\mathbf{k}\uparrow}$ , we obtain mean-field equations where the form factor from right and left side drops out. In summary, we obtain for the  $d$ -wave channel the same gap equation as Eq. (13), but with  $g_0 = 3J\rho(0)/8$ , i.e., there is an effective attraction in the  $d$ -wave channel and the on-site Hubbard repulsion is orthogonal (i.e., the product of  $U$  and the function  $f_d(\mathbf{k})$  exactly averages to zero under a BZ integral). The sign-changing  $d$ -wave pair condensate realizes an order parameter of the form  $\Delta_{\mathbf{k}} = \Delta_0(\cos k_x - \cos k_y)$ . This order parameter  $\Delta_{\mathbf{k}}$  exhibits sign changes (by symmetry) and has nodal lines along the diagonals of the Brillouin zone. If these hit the Fermi surface, it has implications for the low-energy properties of the superconductor, see Fig. 5(d).

The second perspective is guided by knowledge of how typical spin-fluctuation pairing interactions behave: Usually, the interaction is repulsive everywhere, i.e.,  $V(\mathbf{k}, \mathbf{k}') > 0$  for all combinations of  $\mathbf{k}$  and  $\mathbf{k}'$ . This property is also inherited to the singlet interaction,  $V^s(\mathbf{k}, \mathbf{k}') > 0$ , see Eq. (5). Looking now at the mean-field self-consistency equation, Eq. (10), one sees that for an order parameter  $\Delta_{\mathbf{k}}$  that has the same sign everywhere, let us choose it positive  $\Delta_{\mathbf{k}} > 0$ , there is mathematically no solution possible because the l.h.s. is positive for all  $\mathbf{k}$  and the r.h.s. is a

sum of negative terms since  $\tanh(x) > 0$  for  $x > 0$  and  $E_{\mathbf{k}'} > 0$ . Allowing for a sign changing order parameter, there is however the possibility of finding a self-consistent solution if the order parameter  $\Delta_{\mathbf{k}'}$  has a different sign than the order parameter  $\Delta_{\mathbf{k}}$  for pairs of  $\mathbf{k}$  and  $\mathbf{k}'$  where the pairing interaction  $V^s(\mathbf{k}, \mathbf{k}')$  is largest. Indeed, the order parameter needs to be a smooth function of  $\mathbf{k}$  and satisfy the condition  $\Delta_{\mathbf{k}}^s = \Delta_{-\mathbf{k}}^s$  (even parity) such that the momentum sum  $\sum_{\mathbf{k}'}$  sums up positive and negative contributions but still can compensate for the overall minus sign on the r.h.s.

Finally, a remark for the case of triplet superconductivity: Even with a repulsive bare interaction  $V(\mathbf{k}, \mathbf{k}') > 0$ , one sees that the anti-symmetrization in Eq. (5) yields a pairing interaction  $V^{s/t}(\mathbf{k}, \mathbf{k}')$  that is positive for some  $\mathbf{k}$  and  $\mathbf{k}'$  and negative for others (simply from the fact that there is a momentum dependence). However, the order parameter needs to be of odd parity  $\Delta_{\mathbf{k}}^t = -\Delta_{-\mathbf{k}}^t$  so that the order parameter must exhibit a sign change if becoming nonzero.

### 3 Spin fluctuation pairing

#### 3.1 Spin susceptibility

Many unconventional superconducting materials have similar phenomenology in the overall phase diagram, namely that there is a magnetic state close to the superconducting phase, thus suggesting that fluctuations in the vicinity of the magnetic phase can provide the necessary effective pairing interaction because near the magnetic phase boundary the magnetic susceptibility  $\chi(\mathbf{q}, \omega)$  is enhanced [10]. The magnetic susceptibility as quantum mechanical response function is given by the spin-spin correlator  $\langle T_\tau \vec{S}(\mathbf{r}, \tau) \cdot \vec{S}(0, 0) \rangle$  with the spin-operator  $\vec{S}(\mathbf{r}, \tau) = \frac{1}{2} c_{\mathbf{r},\alpha}^\dagger(\tau) \vec{\sigma}_{\alpha\beta} c_{\mathbf{r},\beta}(\tau)$  and the time ordering operator  $T_\tau$  [13]. Parametrizing the components of the spin operator in terms of the raising and lowering operators  $S^\pm = S^x \pm iS^y$ , one can discuss the spin-spin correlator (and therefore the spin susceptibility) in terms of transverse  $\langle S^+ S^- \rangle$  and longitudinal  $\langle S^z S^z \rangle$  parts. Starting from the paramagnetic phase (without spin-orbit coupling), these are identical such that we focus on the transverse part only.

Fourier transformation to momentum space yields

$$\begin{aligned} \chi_0^{+-}(\mathbf{q}, \tau) &= \frac{1}{N} \sum_{\mathbf{k}, \mathbf{k}'} \langle T_\tau S^+(\mathbf{q}, \tau) S^-(\mathbf{-q}, 0) \rangle \\ &= \frac{1}{N} \sum_{\mathbf{k}, \mathbf{k}'} \langle T_\tau c_{\mathbf{k}+\mathbf{q}, \uparrow}^\dagger(\tau) c_{\mathbf{k}, \downarrow}(\tau) c_{\mathbf{k}'-\mathbf{q}, \downarrow}^\dagger(0) c_{\mathbf{k}', \uparrow}(0) \rangle. \end{aligned} \quad (15)$$

The correlator can be calculated using Wick's theorem (note the Fermionic statistics) and expressed in terms of the free Green function  $G_0^\sigma(\mathbf{k}, \tau) = \langle T_\tau c_{\mathbf{k}, \sigma}(\tau) c_{\mathbf{k}, \sigma}^\dagger(0) \rangle$  (for an introduction to the Green function formalism, see for example Ref. [17]). with the result

$$\begin{aligned} \chi_0^{+-}(\mathbf{q}, \tau) &= -\frac{1}{N} \sum_{\mathbf{k}, \mathbf{k}'} \langle T_\tau c_{\mathbf{k}', \uparrow}(0) c_{\mathbf{k}+\mathbf{q}, \uparrow}^\dagger(\tau) \rangle \langle T_\tau c_{\mathbf{k}, \downarrow}(\tau) c_{\mathbf{k}'-\mathbf{q}, \downarrow}^\dagger(0) \rangle \\ &= -\frac{1}{N} \sum_{\mathbf{k}} G_0^\uparrow(\mathbf{k}+\mathbf{q}, -\tau) G_0^\downarrow(\mathbf{k}, \tau). \end{aligned} \quad (16)$$

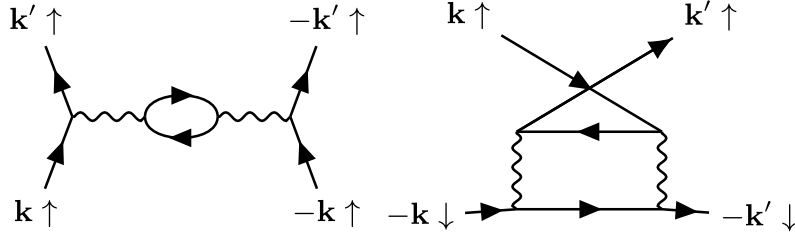


**Fig. 6:** Second order screening (bubble) and exchange (ladder) diagrams. Note that each interaction line  $U$  depicted by a wiggly line connects opposite spins only.

To evaluate the susceptibility, we transform from imaginary time  $\tau$  to Matsubara frequency and introduce the Green functions  $G_0^\sigma(\mathbf{k}, \tau) = \frac{1}{\beta} \sum_{i\omega_n} e^{-i\omega_n \tau} G_0^\sigma(\mathbf{k}, i\omega_n)$  to obtain

$$\chi_0^{+-}(\mathbf{q}, i\nu_n) = \int_0^\beta d\tau e^{i\nu_n \tau} \chi_0^{+-}(\mathbf{q}, \tau) = -\frac{1}{\beta N} \sum_{\mathbf{k}, i\omega_m} G_0^\uparrow(\mathbf{k}+\mathbf{q}, i\omega_m + i\nu_n) G_0^\downarrow(\mathbf{k}, i\omega_m) \quad (17)$$

The Matsubara Green functions of a free electron gas with energy dispersion  $\varepsilon_{\mathbf{k}}$  are given by  $G_0^\sigma(\mathbf{k}, i\omega_m) = 1/(i\omega_m - \varepsilon_{\mathbf{k}})$ , i.e., have poles at  $i\omega_n = \varepsilon_{\mathbf{k}}$  and are independent of spin for the paramagnetic case. Finally, we can evaluate the Matsubara sum over the fermionic frequency  $i\omega_m$  to yield the susceptibility at the bosonic frequency  $i\nu_n$ ,

$$\chi_0^{+-}(\mathbf{q}, i\nu_n) = -\frac{1}{N} \sum_{\mathbf{k}} \frac{n_F(\varepsilon_{\mathbf{k}+\mathbf{q}}) - n_F(\varepsilon_{\mathbf{k}})}{i\nu_n + \varepsilon_{\mathbf{k}+\mathbf{q}} - \varepsilon_{\mathbf{k}}}, \quad (18)$$

that for a paramagnetic metal is identical to the longitudinal one  $\chi_0^{+-}(\mathbf{q}, i\nu_n) = \chi_0^{zz}(\mathbf{q}, i\nu_n)$ . At zero frequency  $i\nu_n = 0$ , one can analyze the conditions for sizeable contributions in the momentum sum: The numerator generates a singularity for the same values of the energy dispersion  $\varepsilon_{\mathbf{k}+\mathbf{q}} = \varepsilon_{\mathbf{k}}$ , but the difference of the Fermi functions  $n_F$  for these arguments are only sizeable if the eigenenergies are close to zero energy (within a window of several  $k_B T$ ), thus there are only contributions from  $\mathbf{k}$  and  $\mathbf{k}+\mathbf{q}$  close to the Fermi surface. Phase space is large if additionally, the respective Fermi velocities  $v_F(\mathbf{k})$  and  $v_F(\mathbf{k}+\mathbf{q})$  are (small and opposite to each other) yielding the argument about Fermi surface nesting for large contributions to the (static) susceptibility/Lindhard function.

### 3.2 Pairing interaction

The interaction from a Hubbard model

$$H_{\text{int}} = U \sum_{\mathbf{r}} c_{\mathbf{r},\uparrow}^\dagger c_{\mathbf{r},\uparrow} c_{\mathbf{r},\downarrow}^\dagger c_{\mathbf{r},\downarrow} = U \sum_{\mathbf{r}} n_{\mathbf{r},\uparrow} n_{\mathbf{r},\downarrow}, \quad (19)$$

can be taken into account in perturbation theory [18] (see Fig. 6) by considering the screening effect due to all other electrons (bubble diagrams, longitudinal) and the exchange of electrons (ladder diagrams, transverse). The effective interaction as already postulated in Eq. (1) is given by

$$V(\mathbf{k}, \mathbf{k}') = U + V_{\text{lo}}^{\text{RPA}}(\mathbf{k}-\mathbf{k}') + V_{\text{tr}}^{\text{RPA}}(\mathbf{k}+\mathbf{k}'). \quad (20)$$

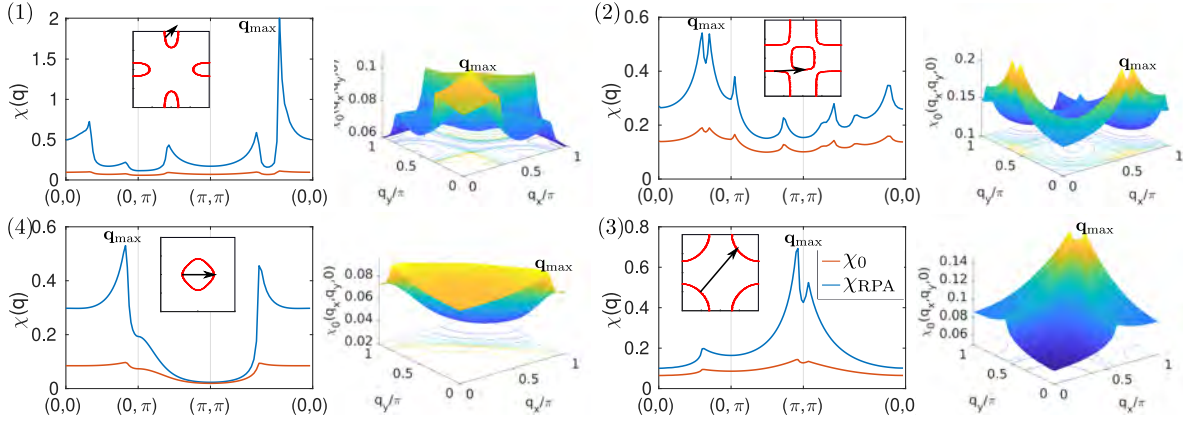


**Fig. 7:** Single band model: susceptibility (red: bare, blue: RPA) at a choice of Hubbard interactions yielding a fixed eigenvalue  $\lambda_1 = 0.1$  for the pairing. (1)–(4) The four representative single band models have quite different structure of the susceptibility with peak structures that are localized (2), (3) or ridges of large susceptibility (1), (4). The maximum of the susceptibility a momentum transfer  $\mathbf{q}_{\text{max}}$  is given by a combination of Fermi surface nesting, density of states properties and available phase space for scattering processes indicated by the black arrow in the inset with the Fermi surface.

The longitudinal contribution is restricted to an even number of bubbles, thus the series only has even powers of  $U$  and can be rewritten in terms of the spin (s) and charge (c) susceptibility,

$$\begin{aligned} V_{\text{lo}}^{\text{RPA}}(\mathbf{k} - \mathbf{k}') &= \frac{U^3 \chi_0^{zz}(\mathbf{k} - \mathbf{k}')^2}{1 - U^2 \chi_0^{zz}(\mathbf{k} - \mathbf{k}')^2} = \frac{U^2}{2} \left( \frac{\chi_0^{zz}(\mathbf{k} - \mathbf{k}')}{1 - U \chi_0^{zz}(\mathbf{k} - \mathbf{k}')} - \frac{\chi_0^{zz}(\mathbf{k} - \mathbf{k}')}{1 + U \chi_0^{zz}(\mathbf{k} - \mathbf{k}')} \right) \\ &= \frac{U^2}{2} (\chi_s(\mathbf{k} - \mathbf{k}') - \chi_c(\mathbf{k} - \mathbf{k}')). \end{aligned} \quad (21)$$

The transverse part is formally given by a geometric series with the transverse susceptibility,

$$V_{\text{tr}}^{\text{RPA}}(\mathbf{k} + \mathbf{k}') = \frac{U^2 \chi_0^{+-}(\mathbf{k} + \mathbf{k}')}{1 - U \chi_0^{+-}(\mathbf{k} + \mathbf{k}')} . \quad (22)$$

Since we are only discussing the paramagnetic case, from now on the difference between transverse and longitudinal susceptibility is dropped. First, we observe that the spin susceptibility exhibits a singularity if  $1 - U \chi_0^{zz}(\mathbf{q}) = 0$ , which signals an instability towards a spin-density wave state if it occurs at finite  $\mathbf{q}$ . It is the usual Stoner instability for an itinerant ferromagnet if it occurs at  $\mathbf{q} = 0$  since the (bare) susceptibility at  $T=0$  and  $\mathbf{q} = 0$  is just the density of states at the Fermi level  $\chi_0^{zz}(0) = \rho(0)$ . Second, close to such a magnetic phase, the spin fluctuations are strong and the effective pairing interaction becomes large as well. Ignoring the charge fluctuations (which in this approximation do not become dominant because of the  $1 + U \chi_0^{zz}(\mathbf{q})$  denominator), one sees that the spin susceptibility (and consequently the pairing interaction) is a monotonous function of  $U$ , i.e., large values of  $\chi_0^{zz}(\mathbf{q})$  lead to large values of  $\chi_s(\mathbf{q})$ . Consequently, to identify dominant contributions for pairing and qualitatively understand the solutions  $\Delta_{\mathbf{k}}$  of the self-consistence equation Eq. (10), it is sufficient to look for peaks in the bare susceptibility (Lindhard function).

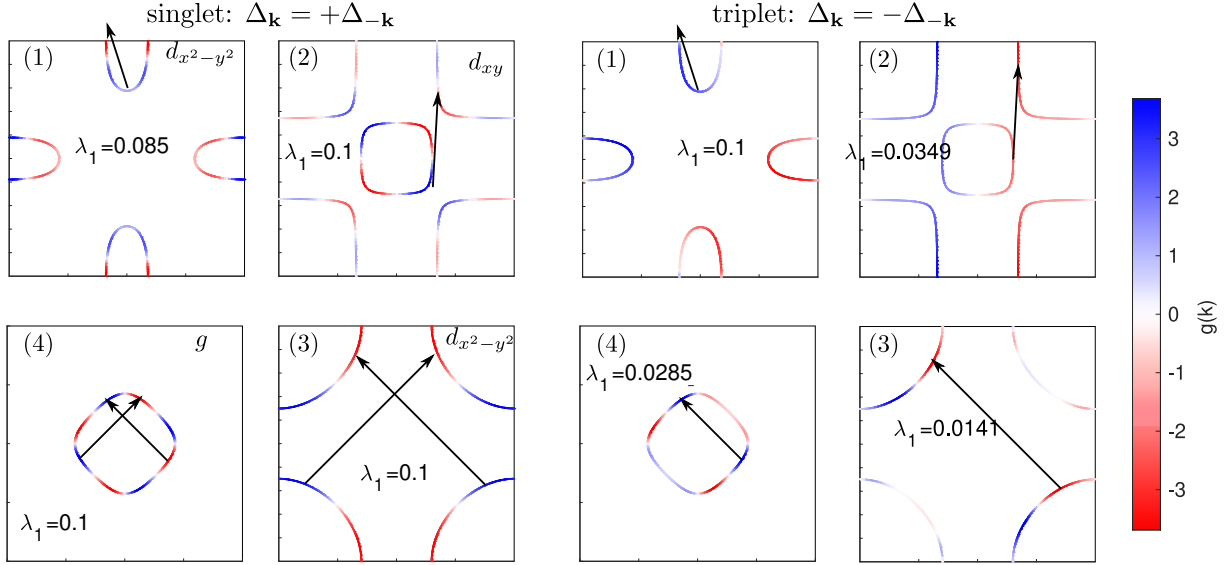


**Fig. 8:** Single band model: superconducting order parameter calculated using Eq. (11) from the spin-fluctuation pairing interaction in Eq. (20). Solutions of the linearized gap equation for the four representative models (1)–(4), compare Fig. 4 with bare interaction  $U$  tuned such that the leading instability has  $\lambda = 0.1$ . Arrows indicate dominant peaks in the bare susceptibility as shown in Fig. 7. For singlet states, these connect order parameters of different sign while for the triplet states, the dominant pair scattering connects between parts where the order parameter has the same sign.

### 3.3 Single band model

In the following, we discuss a couple of examples of simple band structures, the properties of the susceptibility and expected superconducting pairing states. The starting point is a single-band model with one  $d_{x^2-y^2}$  orbital as discussed in view of the cuprate superconductors. The model is given already in Eq. (2) and is parametrized by the nearest neighbor hopping  $t$ , the next-nearest-neighbor hopping  $t'$  and the chemical potential  $\mu$ . In the following we assume the chemical potential to be tuned such that a given (spin-summed) density  $\langle n \rangle$  is achieved. This model allows four different Fermi surface topologies, see Fig. 4 and therefore also different nesting conditions with differences in the Lindhard function (susceptibility), see Fig. 7. The dominant peaks in the susceptibility are then responsible for the momentum structure of the superconducting order parameter. For singlet pairing  $\mathbf{q}_{\max}$  connects Fermi surface points where the order parameter is maximum and has opposite sign, while for solutions in the triplet channel, the pairing interaction is negative and largest for this momentum transfer and consequently  $\mathbf{q}_{\max}$  connects order parameter of the same sign as illustrated in Fig. 8.

Given the three Lifshitz transition lines for the single band model, the Fermi surface topology is already very different in each regime and allows for pairing states of all possible symmetries, see Fig. 9. Indeed, there are also triplet instabilities either close to the van Hove filling where the density of states is large or in the regime of small Fermi energy where the band structure

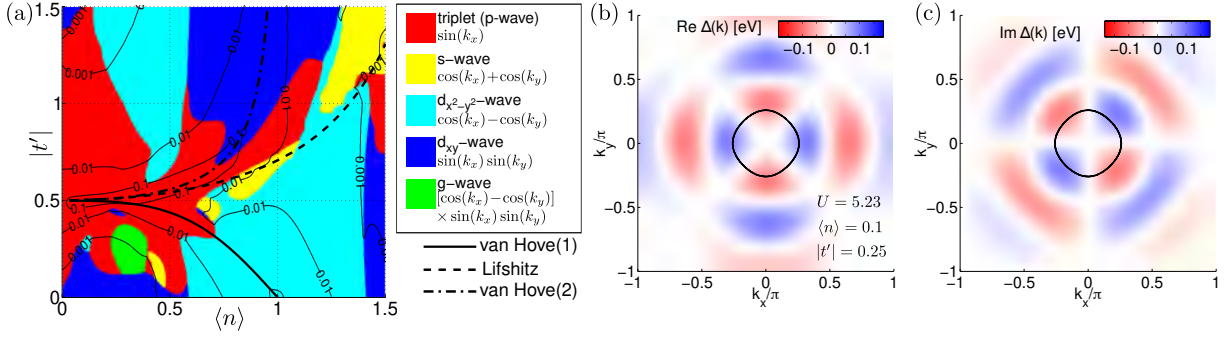


**Fig. 9:** (a) Superconducting phase diagram from spin-fluctuations showing the superconducting instabilities of the one band model in the limit of small interactions  $U = 0.08$ . Lines indicate eigenvalue  $\lambda$  of the leading instability. (b) At small filling (Fermi surface indicated by black circle), spin-fluctuation theory predicts a time-reversal symmetry breaking  $d_{x^2-y^2} + id_{xy}$  superconducting instability as worked out by a self-consistent Bogoliubov-de-Gennes calculation based on Eq. (10) [21].

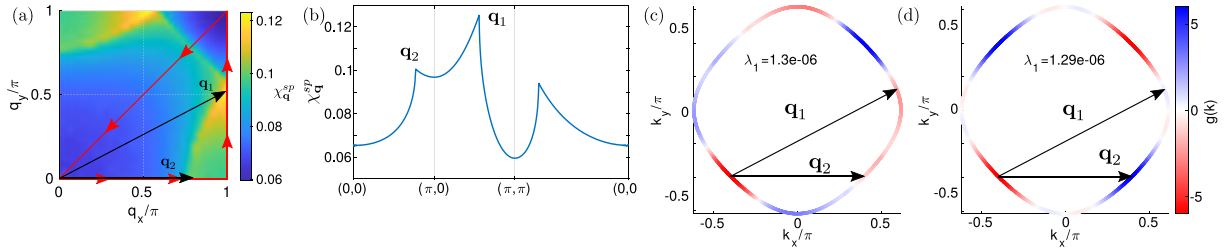


**Fig. 10:** Triplet pairing from spin fluctuations at finite momentum in the single band Hubbard model: (a) The spin susceptibility ( $U = 0.05$ ,  $t = 1$ ,  $t' = 0$ ,  $n = 0.54$ ,  $T = 0.0001$ ) exhibits two dominant peaks at  $\mathbf{q}_1$  and  $\mathbf{q}_2$ . (b) Linear plot along a high symmetry path. Gap symmetry function  $g(\mathbf{k})$  of the leading triplet instability (c) and leading singlet instability (d) showing that the dominant scattering vectors connect parts where the order parameter is large [19].

resembles a parabolic band which has been discussed to exhibit an instability in the triplet channel (at weak coupling). In this case, the pairing state is a  $p_{x,y}$  state with momentum dependence  $\propto \sin k_x$  or  $\propto \sin k_y$ . If the susceptibility is peaked at a finite  $\mathbf{q}_{\max}$ , the pairing instabilities tend to be dominated by singlet states, but there is the possibility to take advantage of the spin fluctuations even in the triplet channel if  $\mathbf{q}_{\max}$  spans multiple nodes and the Fermi surface topology is susceptible for those pairing states with higher order harmonics, see Fig. 10 [19].

To conclude this section on spin-fluctuations in a single band Hubbard model, we want to stress that the approach presented here is based on a perturbative expansion of the pairing interaction in powers of  $U$ . It is strictly correct only in the weak coupling regime and to order  $U^3$  since in the RPA approach, only certain types of diagrams are summed over. Still it seems to connect smoothly to numerically exact and unbiased calculations in the strong coupling regime for the mentioned single band model [20].

### 3.4 Multiband generalization

A number of unconventional superconductors cannot be described by a single band model because of multiple atoms in the elementary cell and/or a crystal field splitting such that multiple orbital degrees of freedom have to be considered for the relevant low-energy electronic structure. Prominent material examples are the Fe-based superconductors where all five Fe- $d$  states contribute to the electronic structure [22, 12], in  $\text{Sr}_2\text{RuO}_4$  three orbital degrees of freedom are important [23], the nickelate systems (with one or more layers) [11, 24] and the kagome systems where three sublattice degrees of freedom are in the elementary cell [9].

In the case of multiorbital systems, the normal state Hamiltonian can be written in a tight-binding model as

$$H_0 = \sum_{\mathbf{k}\sigma\ell\ell'} t_{\mathbf{k}}^{\ell\ell'} c_{\ell\sigma}^\dagger(\mathbf{k}) c_{\ell'\sigma}(\mathbf{k}), \quad (23)$$

where  $t_{\mathbf{k}}^{\ell\ell'} = \sum_{\delta} t_{\delta}^{\ell\ell'} \exp(i\mathbf{k} \cdot \delta)$  is the Fourier transform of the hopping elements connecting orbital  $\ell$  with orbital  $\ell'$  at distance  $\delta$ .

A unitary transformation with the matrix elements  $a_{\mu}^{\ell}(\mathbf{k})$  diagonalizes the Bloch Hamiltonian such that it becomes

$$H_0 = \sum_{\mathbf{k}\sigma\mu} \varepsilon_{\mu,\mathbf{k}} c_{\mu\sigma}^\dagger(\mathbf{k}) c_{\mu\sigma}(\mathbf{k}) \quad (24)$$

with eigenenergies  $\varepsilon_{\mu,\mathbf{k}}$  and  $c_{\mu\sigma}^\dagger(\mathbf{k})$  is the operator creating an electron in Bloch state of band  $\mu$  at momentum  $\mathbf{k}$ . In Fig. 11(e,f) the electronic structure of such a five band model is illustrated for the example of  $\text{LiFeAs}$ . This model has been derived from an ab-initio calculation in Ref. [26] by restricting to the  $k_z = 0$  plane. The model of  $\text{K}_x\text{Fe}_2\text{Se}_2$  (g,h) only has electronlike pockets. For completeness and later reference, we also cite the generalization of the Hubbard interaction Eq. (19) to multiple orbitals as usually discussed in terms of a Hubbard-Kanamori form,

$$H_{\text{int}} = U \sum_{i,\ell} n_{i\ell\uparrow} n_{i\ell\downarrow} + U' \sum_{i,\ell'<\ell} n_{i\ell} n_{i\ell'} + J \sum_{i,\ell'<\ell} \sum_{\sigma,\sigma'} c_{i\ell\sigma}^\dagger c_{i\ell'\sigma'}^\dagger c_{i\ell\sigma'} c_{i\ell'\sigma} + J' \sum_{i,\ell' \neq \ell} c_{i\ell\uparrow}^\dagger c_{i\ell\downarrow}^\dagger c_{i\ell\downarrow} c_{i\ell'\uparrow}, \quad (25)$$

where the parameters  $U$ ,  $U'$ ,  $J$ ,  $J'$  are related by  $U' = U - 2J$ , and  $J = J'$  in the spin-rotational invariant case, i.e., two parameters  $U$  and  $J/U$  parametrize the interactions [28, 29].

If the additional degree of freedom is a sublattice, the interaction might need to be complemented by nearest neighbor Coulomb interactions (for a single orbital model)

$$H_V = V \sum_{\substack{ij \\ \mu\sigma\sigma'}} n_{\alpha,i,\sigma} n_{\bar{\alpha},j,\sigma'}, \quad (26)$$

where  $\alpha$  denotes a sublattice and  $\bar{\alpha}$  is a sublattice distinct from  $\alpha$ . We are not elaborating on this further here, more details can be found for example in Ref. [30].

For a multiband model, the analog of the paramagnetic susceptibility, Eq. (17) is given by

$$\chi_{\ell_1\ell_2\ell_3\ell_4}^0(\mathbf{q}, i\nu_n) = - \sum_{\mathbf{k}, i\omega_n} G^{\ell_1\ell_3}(\mathbf{k}+\mathbf{q}, i\omega_n + i\nu_n) G^{\ell_2\ell_4}(\mathbf{k}, i\omega_n) \quad (27)$$

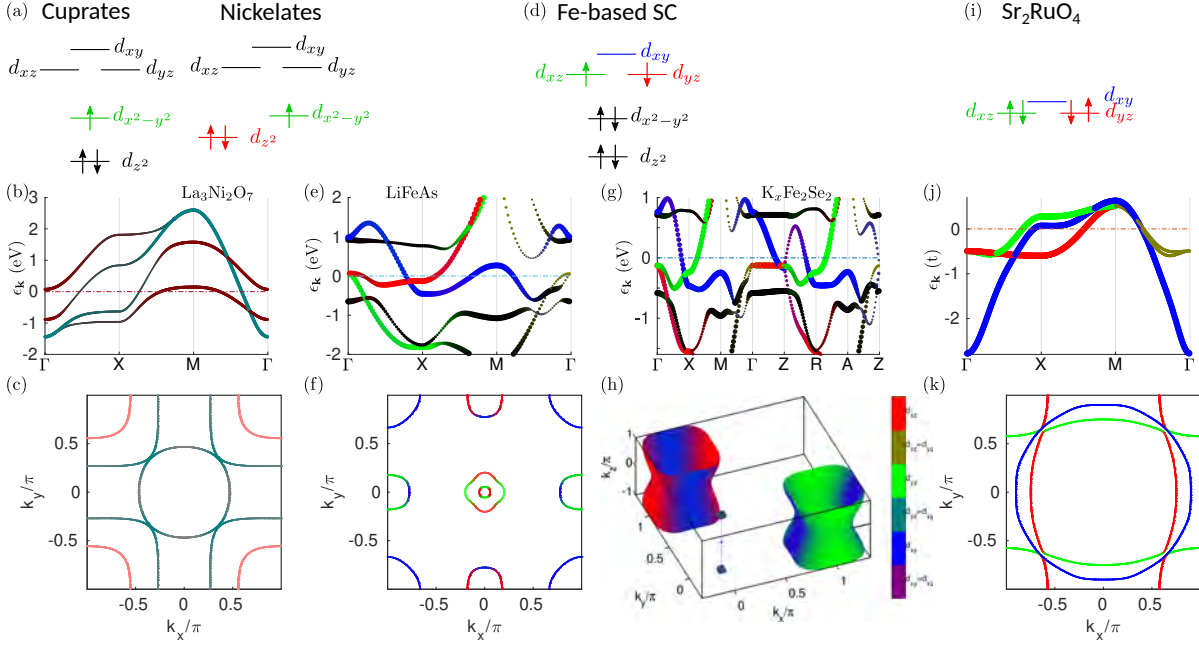


**Fig. 11:** Examples of electronic structure of multiband superconductors (a) Sketch of crystal field splitting for cuprate and nickelate systems (b) Band structure of a bilayer nickelate [25] (c) corresponding Fermi surface with  $d_{z^2}$  and  $d_{x^2-y^2}$  orbital character. (d) Fe-based systems exhibiting the three  $t_{2g}$  orbitals at the Fermi level. (e) Band structure of a model for LiFeAs [26] and (f) corresponding Fermi surface with electron pockets at X and Y point and holelike pockets at the  $\Gamma$  point and M point. (g) Electronic structure of a 122 system with sizeable dispersion along  $k_z$  exhibiting only electronlike pockets at the X and Y point for  $K_x\text{Fe}_2\text{Se}_2$  [27]. (i) Three relevant orbital states in  $\text{Sr}_2\text{RuO}_4$  yield three bands (j) and three Fermi sheets (k).

where the Green functions can be expressed in spectral representation

$$G^{\ell_1\ell_2}(\mathbf{k}, i\omega_n) = \sum_{\mu} \frac{a_{\nu}^{\ell_1}(\mathbf{k})a_{\nu}^{\ell_2,*}}{i\omega_n - \varepsilon_{\mu,\mathbf{k}}}. \quad (28)$$

Again, we can perform the frequency sum analytically and obtain the generalized Lindhard function

$$\chi_{\ell_1\ell_2\ell_3\ell_4}^0(\mathbf{q}, i\nu_n) = - \sum_{\mathbf{k}, \mu, \nu, i\omega_n} \frac{a_{\nu}^{\ell_4}(\mathbf{k})a_{\nu}^{\ell_2,*}(\mathbf{k})a_{\mu}^{\ell_1}(\mathbf{k}+\mathbf{q})a_{\mu}^{\ell_3,*}(\mathbf{k}+\mathbf{q})(n_F(\varepsilon_{\mu,\mathbf{k}+\mathbf{q}}) - n_F(\varepsilon_{\nu,\mathbf{k}}))}{i\nu_n + \varepsilon_{\mu,\mathbf{k}+\mathbf{q}} - \varepsilon_{\nu,\mathbf{k}}}. \quad (29)$$

To calculate the effective pairing interaction from a spin-fluctuation mechanism, the RPA approach needs to be generalized to a matrix expression [22, 29]

$$\chi_{s/c\ell_1\ell_2\ell_3\ell_4}^{\text{RPA}}(\mathbf{q}, \omega) = \left( \chi^0(\mathbf{q}, \omega) (1 \mp \bar{U}^{s/c} \chi^0(\mathbf{q}, \omega))^{-1} \right)_{\ell_1\ell_2\ell_3\ell_4}, \quad (30)$$

where the interaction matrices  $\bar{U}^{s,c}$  contain the bare interactions parametrized by  $U$ ,  $U'$ ,  $J$  and  $J'$  and become momentum dependent in the presence of nearest-neighbor Coulomb interactions, Eq. (26).

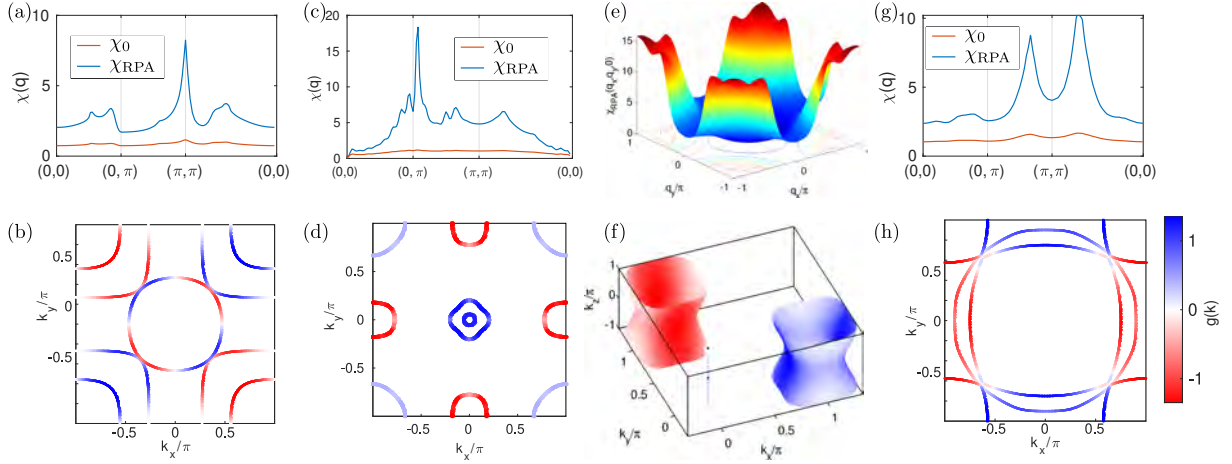


**Fig. 12:** Examples of superconducting pairing in multiband systems. (a) Susceptibility and (b) pairing state of a bilayer nickelate exhibiting a d-wave state. (c) Susceptibility for LiFeAs and (d) corresponding leading  $s_{\pm}$  pairing state with full gap. (e) Susceptibility as calculated from a model of  $\text{K}_x\text{Fe}_2\text{Se}_2$  that only exhibits electronlike pockets and has a d-wave instability (f). The susceptibility of  $\text{Sr}_2\text{RuO}_4$  using a band structure from a plain DFT calculation sustains a d-wave instability (h).

The generalization of the pairing interaction (in orbital representation) is then given by

$$\Gamma_{\ell_1\ell_2\ell_3\ell_4}(\mathbf{k}, \mathbf{k}') = \frac{1}{2} \left( 3\bar{U}^s \chi_s^{\text{RPA}}(\mathbf{k}-\mathbf{k}') \bar{U}^s + \bar{U}^s - \bar{U}^c \chi_c^{\text{RPA}}(\mathbf{k}-\mathbf{k}') \bar{U}^c + \bar{U}^c \right)_{\ell_1\ell_2\ell_3\ell_4} \quad (31)$$

and enters the self-consistent equation (analogous to Eq. (10)) with a symmetrized and antisymmetrized pairing interaction.

Taking the limit  $T \rightarrow T_c$ , only the states on the Fermi surface become relevant. In that process, the pairing interaction is projected to band space such that the pairing vertex in band space

$$\Gamma_{\nu\mu}(\mathbf{k}, \mathbf{k}') = \text{Re} \sum_{\ell_1\ell_2\ell_3\ell_4} a_{\nu}^{\ell_1,*}(\mathbf{k}) a_{\nu}^{\ell_4,*}(-\mathbf{k}) \Gamma_{\ell_1\ell_2\ell_3\ell_4}(\mathbf{k}, \mathbf{k}') a_{\mu}^{\ell_2}(\mathbf{k}') a_{\mu}^{\ell_3}(-\mathbf{k}') \quad (32)$$

enters the linearized gap equation, Eq. (11). Note that the band index on the r.h.s. is formally a dummy index since the knowledge of  $\mathbf{k}$  and  $\mathbf{k}'$  on the Fermi surface automatically fixes the band indices  $\mu$  and  $\nu$ . We note that the pairing interaction in Eq. (31) is dominated by momentum transfer  $\mathbf{k} \pm \mathbf{k}'$  where the susceptibility is peaked and is dominated by inter-orbital contributions since for those the susceptibility tends to be large and the bare interaction  $\bar{U}^{s,c}$  is larger for these processes as well. Still, we note that dominant Hund's pairing [31, 32], i.e., when  $U' = U - 2J$  becomes negative can induce large inter-orbital pairing and some combinations of the pairing interaction can become negative as discussed in Ref. [29] to drive inter-orbital pairing together with intra-orbital pairing. In Fig. 12 some examples of pairing in multiband models are shown where the dominant mechanism can be understood from the structure of the spin susceptibility

$$\chi_{\text{phys}}(\mathbf{q}) = \frac{1}{2} \sum_{\ell\ell'} \chi_{\ell\ell'}(\mathbf{q}). \quad (33)$$

**Interplay of Fermi surface geometry and nesting** We now discuss some representative example materials; the choice is done for illustration purposes only and does not claim to be complete in any way. The nickelate superconductors have been proposed as a sister compound to the cuprates [24], but only recently, it was possible to actually obtain superconducting infinite layer nickelates in thin films or bilayer nickelates that are found to be superconducting under moderate pressure [33]. The common theme for the superconducting mechanism is thought to be similar to the cuprates. However, there are several differences such as the different crystal field splitting (see Fig. 11(a)), i.e., multiple orbitals are relevant for the low energy electronic structure or the question of dispersion in the third direction as evidenced from a smaller anisotropy in transport. For the superconducting instability, some investigations point towards a  $d$ -wave state in analogy to single band cuprates. Taking into account correlations, there might be a competing  $s$ -wave instability; the same trend is also found in models for bilayer nickelates; depending on the details either a sign-changing  $s$ -wave or  $d$ -wave instability seems favorable (see Fig. 11(b)) [25, 34]. For the Fe-based superconductors, calculations using the spin-fluctuation pairing mechanism find competing  $s_{\pm}$  states for the prototype Fermi surface (see Fig. 11(d)) [26], but different Fermi surface topologies as found in strongly doped  $K_x\text{Fe}_2\text{Se}_2$  [27] of the monolayer FeSe with large  $T_c$  would favor a  $d$ -wave instability with sign change between the electronlike Fermi surfaces. The case of  $\text{Sr}_2\text{RuO}_4$  has been under intense investigation in the last two decades. Early evidence for spin triplet superconductivity from NMR Knight shifts sparked large interest in the compound and led to theoretical investigations of how to stabilize such an instability. More experimental efforts using NMR revealed that there was a technical challenge that was overcome in a later experiment finding a suppression of the spin susceptibility in the superconducting state, a clear evidence for spin singlet superconductivity; the same conclusions were also drawn from data for the specific heat in a magnetic field. The exact nature of the superconducting order parameter is still under debate, both experimentally and theoretically [23]. Reconciling all experimental data with one single proposal for the superconducting state seems not possible, but a plain calculation for spin-fluctuation driven superconductivity starting from an ab-initio band structure points to a  $d$ -wave instability, see Fig. 12(h).

### 3.5 Sublattice degree of freedom and kagome systems

The calculation of the susceptibility and consequently also the pairing interaction for systems with multiple lattice points per elementary cell needs some additional care. Relevant examples in view of unconventional superconductors are Fe-based systems of the 122 structure, where no exact downfolding to a five band model with only one Fe per elementary cell exists (more reading on this in Chapter 6 in Ref. [35]) or the kagome systems where three sublattices are needed, see Fig. 1.

The underlying concept can be understood by examining electrons on a one dimensional chain. For calculating the (bare) susceptibility in this system, we start with the dispersion

$$\varepsilon_k = -2t \cos ka, \quad (34)$$

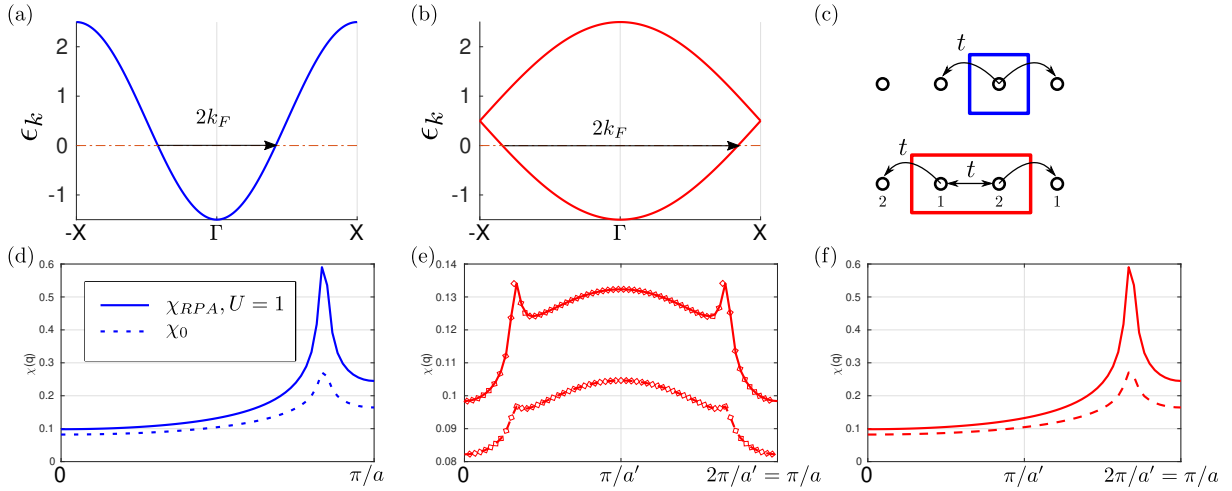


**Fig. 13:** Susceptibility and sublattice degree of freedom: (a) Bandstructure of a 1d nearest neighbor tight-binding model (b) same model, but described with two identical sublattices. (c) Description of the same physical system with one lattice point per elementary cell (blue) and two lattice points per elementary cell (red) where intra-unit cell hoppings (straight lines) and inter-unit cell hoppings (curved lines) are present. (d) Paramagnetic susceptibility at  $\mu = -0.5t$ . (e) Paramagnetic susceptibility from Eq. (27) calculated in the basis where the Hamiltonian is periodic in the BZ, (f) same, but including the effect of the unitary transformation, Eq. (35).

and use Eq. (18). Indeed, the Bloch Hamiltonian is just  $\varepsilon_k$  and periodic in the Brillouin zone  $\varepsilon_k = \varepsilon_{k+2\pi/a}$  and it becomes obvious that the susceptibility  $\chi_0^{+-}(\mathbf{q}, i\nu_n)$  is also periodic with the reciprocal lattice vector  $\chi_0^{+-}(q, i\nu_n) = \chi_0^{+-}(q+2\pi/a, i\nu_n)$ . To illustrate the effect of a sublattice, we now use a different elementary cell (that is not a primitive elementary cell) to perform the same calculation. Defining a two sublattice system, the Bloch Hamiltonian becomes a  $2 \times 2$  matrix as

$$\tilde{H}(k) = -t \begin{pmatrix} 0 & 1 + \exp(ik/a') \\ 1 + \exp(-ik/a') & 0 \end{pmatrix}. \quad (35)$$

Now, the lattice constant is  $a' = 2a$  and there are intra unit cell hopping processes that do not acquire a momentum dependence, see Fig. 13(c). We note that the Brillouin zone is now smaller  $(-\pi/a' \cdot \pi/a']$ , still the Hamiltonian is periodic with a reciprocal vector  $\tilde{H}_k = \tilde{H}_{k+\pi/a'}$  and so is the susceptibility  $\chi_{\ell_1 \ell_2 \ell_3 \ell_4}^{+-}(q, i\nu_n) = \chi_{\ell_1 \ell_2 \ell_3 \ell_4}^{+-}(q+2\pi/a, i\nu_n)$ . However, this result does not agree with the susceptibility as calculated using the primitive elementary cell, see Fig. 13(e). The reason is because the Bloch Hamiltonian does not “know” anything about the internal position of the two sublattice states. A way out is to work in a different basis that is connected to the current one by the unitary transformation

$$U = \begin{pmatrix} 1 & 0 \\ 0 & \exp(ika'/2) \end{pmatrix} \quad (36)$$

such that the Bloch Hamiltonian is now

$$H(k) = -t \begin{pmatrix} 0 & 2 \cos(ka'/2) \\ 2 \cos(ka'/2) & 0 \end{pmatrix}, \quad (37)$$

which has the same eigenvalues as  $\tilde{H}_k$ , but the eigenvectors are different and are not periodic with a reciprocal lattice vector since also the Hamiltonian is not  $H_k \neq H_{k+2\pi/a'}$ . The susceptibility calculated following Eq. (27) using this Hamiltonian is periodic with two reciprocal lattice vectors,  $\chi_{\ell_1\ell_2\ell_3\ell_4}^{+-}(q, i\nu_n) = \chi_{\ell_1\ell_2\ell_3\ell_4}^{+-}(q+4\pi/a', i\nu_n) = \chi_{\ell_1\ell_2\ell_3\ell_4}^{+-}(q+2\pi/a, i\nu_n)$  which is the reciprocal lattice vector of the original (primitive) setting. Thus, calculating the physical susceptibility using Eq. (33) one indeed obtains the same result as in the primitive setting. Note that the susceptibilities in the two basis settings of the Hamiltonian are related by just the multiplication of a phase factor  $\exp(\pm i\mathbf{q}/2)$  for the off-diagonal elements that connect the two sublattices as one can easily show from the relation of the eigenvectors in the two settings and the possibility to factor these from the momentum sum in Eq. (27).

**Kagome lattice** For a concrete example where the sublattice degree qualitatively enters the susceptibility calculation and therefore is important for calculations of superconducting pairing, we consider a model on the kagome lattice. This is motivated by the recent discovery of superconductivity in kagome materials [9] where the nature of the superconducting order parameter is currently under debate.

We start from a minimal tight-binding model with only nearest neighbor hoppings such that the Hamiltonian is given by

$$\mathcal{H}_0 = \sum_{\mathbf{k}, \sigma} \psi_{\mathbf{k}\sigma}^\dagger H_0(\mathbf{k}) \psi_{\mathbf{k}\sigma}, \quad (38)$$

where  $\psi_{\mathbf{k}\sigma} = (c_{\mathbf{k}\sigma A}, c_{\mathbf{k}\sigma B}, c_{\mathbf{k}\sigma C})^T$  is a vector containing fermionic operators for the three sublattices and the Bloch Hamiltonian

$$H_0(\mathbf{k}) = - \begin{pmatrix} \mu & t \cos k_3 & t \cos k_1 \\ t \cos k_3 & \mu & t \cos k_2 \\ t \cos k_1 & t \cos k_2 & \mu \end{pmatrix}. \quad (39)$$

The momenta  $k_n = \mathbf{k} \cdot \mathbf{a}_n$  are parametrized with help of the vectors  $\mathbf{a}_1 = (1, 0)/2$ ,  $\mathbf{a}_2 = (1, \sqrt{3})/4$  and  $\mathbf{a}_3 = (-1, \sqrt{3})/4$  connecting to the nearest neighbors.  $\mu$  is the chemical potential and  $t$  the NN hopping integral. The Hamiltonian is diagonalized by a unitary transformation,  $u_{n\alpha}^*(\mathbf{k}) H_{0,\alpha\beta}(\mathbf{k}) u_{\beta m}(\mathbf{k}) = \varepsilon_{n,\mathbf{k}} \delta_{nm}$  yielding the band energies  $\varepsilon_{n,\mathbf{k}}$  and the eigenstates  $u_{n\alpha}(\mathbf{k})$  of band  $n$ . The unitary transformation

$$T(\mathbf{k}) = \begin{pmatrix} e^{-ik_1} & 0 & 0 \\ 0 & e^{-ik_2} & 0 \\ 0 & 0 & 1 \end{pmatrix} \quad (40)$$

transforms the Hamiltonian into a basis which is periodic in the first BZ,

$$\tilde{H}_0(\mathbf{k}) = - \begin{pmatrix} \mu & t(1+e^{2ik_3}) & t(1+e^{-2ik_1}) \\ t(1+e^{-2ik_3}) & \mu & t(1+e^{-2ik_2}) \\ t(1+e^{2ik_1}) & t(1+e^{2ik_2}) & \mu \end{pmatrix} \quad (41)$$

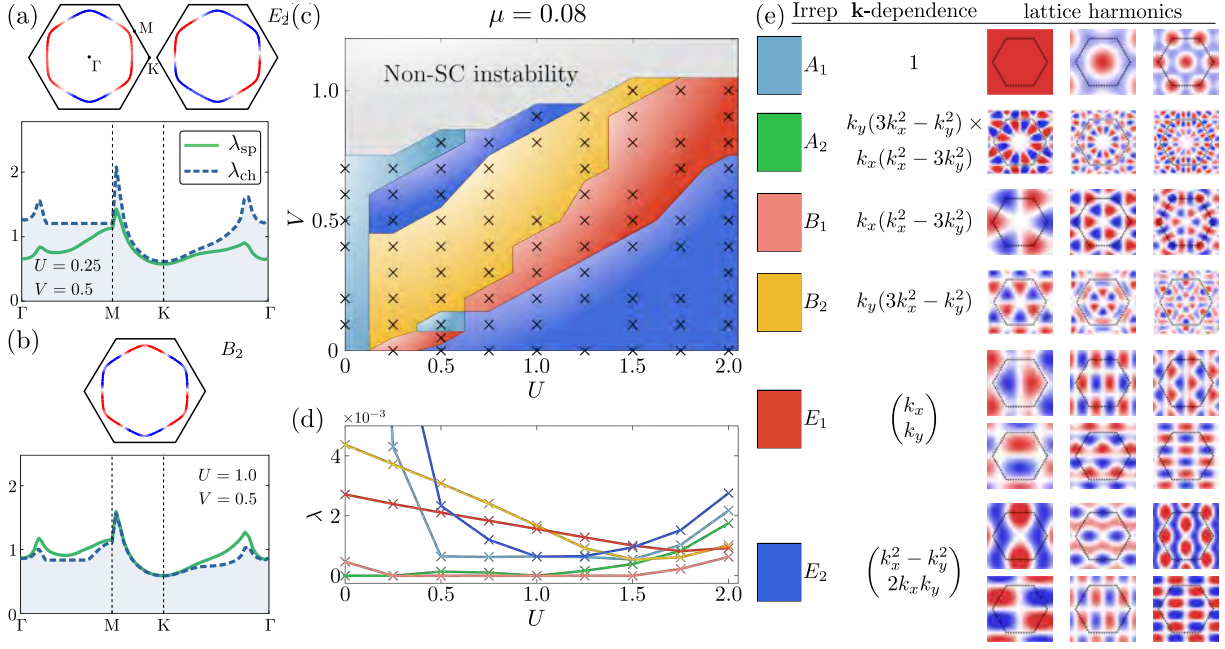


**Fig. 14:** Superconducting instabilities in a kagome system from spin fluctuations including NN Coulomb interactions. Leading superconducting instability driven by spin (a) and charge (b) fluctuations (plotted along high symmetry path). (c) Phase diagram exhibiting many competing superconducting instabilities as revealed from the calculation of the eigenvalue of the linearized gap equation Eq. (11). (e) Labeling for the phase diagram and momentum structure of the SC instabilities [30].

to be used to evaluate the momentum integral in Eq. (29) and the elements of the unitary transformation  $T(\mathbf{k})$  to be used for calculating the susceptibility in the other basis setting,

$$\chi_{0,\alpha\beta}^{+-}(\mathbf{q}, \omega) = \begin{pmatrix} \tilde{\chi}_{0,AA}^{+-} & e^{i(q_2 - q_1)} \tilde{\chi}_{0,AB}^{+-} & e^{-iq_1} \tilde{\chi}_{0,AC}^{+-} \\ e^{i(q_1 - q_2)} \tilde{\chi}_{0,BA}^{+-} & \tilde{\chi}_{0,BB}^{+-} & e^{-iq_2} \tilde{\chi}_{0,BC}^{+-} \\ e^{iq_1} \tilde{\chi}_{0,CA}^{+-} & e^{iq_2} \tilde{\chi}_{0,CB}^{+-} & \tilde{\chi}_{0,CC}^{+-} \end{pmatrix}, \quad (42)$$

where  $\tilde{\chi}_{0,\alpha\beta}^{+-}(\mathbf{q}, \omega)$  is the spin susceptibility evaluated using  $\tilde{H}_0(\mathbf{k})$ , and  $q_n = \mathbf{q} \cdot \mathbf{a}_n$ .

**Superconductivity from spin fluctuations on the kagome lattice** Fig. 14(a,b) show the (eigenvalues of the) susceptibility for the kagome lattice at  $\mu = 0.08$ . Nearest neighbor interactions according to Eq. (26) are taken into account making the charge fluctuations sizeable. Consequently, superconducting instabilities of many symmetries are expected as shown in the phase diagram (c). Looking at the phase diagram, one finds a significant parameter space at sizeable  $U$ , but moderate  $V$  where the  $E_2$ , i.e., a  $d$ -wave type solution is favorable. Generically, the two orthogonal solutions exhibit the same  $T_c$  and therefore condense at the same temperature with two possible settings: Either a real combination of the order parameter is stable, i.e.,  $d+d$  where an additional crystal symmetry is broken when entering the superconducting state, or the order parameters form a complex linear combination  $d+id$ . For an extended discussion on time reversal symmetry breaking in superconductors, see the reviews in Refs. [36, 37]. In the latter

case, the time reversal symmetry is broken in the superconducting state and for the given Fermi surface, the quasiparticle spectrum becomes fully gapped since the nodes of the two states do not coincide. The second case usually lowers the condensation energy and is generically favored see appendix in Ref. [38]. This state would also be consistent with some observations in the kagome materials, namely the full gap as seen in tunneling spectra [39] and evidence for time reversal symmetry breaking in the superconducting state [40]. The latter could also arise from other mechanisms such as loop currents in a complex charge density wave, indicated by the presence of other instabilities in these materials occurring at higher transition temperatures.

## 4 Spectroscopic probes

In this section, we will theoretically analyze properties of unconventional superconductors and point out qualitative differences in a set of spectroscopic probes that can be used to experimentally distinguish between conventional and unconventional superconductors and deduce possible gap symmetries.

To accomplish this task, we first formulate BCS theory in terms of Green functions and then derive physical observables. For a mean-field Hamiltonian of the form of Eq. (6), we can rewrite it in the form

$$H_{\text{MF}} = \sum_{\mathbf{k}} \Psi_{\mathbf{k}}^{\dagger} \hat{H}_{\text{BdG}}(\mathbf{k}) \Psi_{\mathbf{k}}, \quad (43)$$

where we introduced the matrix of the Bogoliubov de Gennes Hamiltonian (BdG)

$$\hat{H}_{\text{BdG}}(\mathbf{k}) = \begin{pmatrix} h(\mathbf{k}) & \Delta^{s/t}(\mathbf{k}) \\ \Delta(\mathbf{k})^{s/t\dagger} & -h(-\mathbf{k})^T \end{pmatrix}, \quad (44)$$

and  $\Psi_{\mathbf{k}}^{\dagger} = (c_{\mathbf{k}\uparrow}^{\dagger}, c_{-\mathbf{k}\downarrow})$ . For a single band model, we have  $h(\mathbf{k}) = \varepsilon_{\mathbf{k}}$  and  $\Delta^{s/t}(\mathbf{k}) = \Delta_{\mathbf{k}}^{s/t}$ , while for the multiband case, the operator runs over all auxiliary quantum numbers that can be orbital or sublattice  $c_{\mathbf{k},\sigma}^{\dagger} = (c_{\mathbf{k}\sigma 1}^{\dagger}, c_{\mathbf{k}\sigma 2}^{\dagger}, \dots)$ . The retarded Green function that formally solves the Schrödinger equation is given by

$$\hat{G}^{(0)}(\mathbf{k}, \omega) = \left( (\omega + i\eta)\mathbb{1} - \hat{H}_{\text{BdG}}(\mathbf{k}) \right)^{-1} = \begin{pmatrix} G_{11}^{(0)}(\mathbf{k}, \omega) & G_{1\bar{1}}^{(0)}(\mathbf{k}, \omega) \\ G_{\bar{1}1}^{(0)}(\mathbf{k}, \omega) & G_{\bar{1}\bar{1}}^{(0)}(\mathbf{k}, \omega) \end{pmatrix}, \quad (45)$$

where we introduced the normal or anomalous parts of the Green function with the notation of  $11$  and  $1\bar{1}$ . For the single band case, the matrix inversion can be done analytically giving the  $2 \times 2$  matrix

$$\hat{G}^{(0)}(\mathbf{k}, \omega) = \frac{(\omega + i\eta)\tau_0 + \varepsilon_{\mathbf{k}}\tau_3 + \Delta_{\mathbf{k}}^{s/t}\tau_1}{(\omega + i\eta)^2 - \varepsilon_{\mathbf{k}}^2 - (\Delta_{\mathbf{k}}^{s/t})^2} \quad (46)$$

with the usual Pauli matrices  $\tau_i$  and the unit matrix  $\tau_0$ .

## 4.1 Density of states

The quasiparticle density of states is then given by

$$\rho_s(\omega) = -\frac{1}{\pi} \text{Tr Im } \widehat{G}^{(0)}(\mathbf{k}, \omega), \quad (47)$$

and the electronic density of states relevant for tunneling is given by

$$\rho(\omega) = -\frac{1}{\pi} \text{Tr Im } G_{11}^{(0)}(\mathbf{k}, \omega) = -\frac{1}{2\pi} \text{Tr Im } (G_{11}^{(0)}(\mathbf{k}, \omega) + G_{\bar{1}\bar{1}}^{(0)}(\mathbf{k}, -\omega)), \quad (48)$$

where the trace is over the auxiliary degrees of freedom (orbital, sublattice) and a sum over momentum  $\mathbf{k}$ . With the help of the unitary transformation in Eq. (7), one can obtain the spectral representation of the Green function that contains products of the matrix elements of the Bogoliubov transformation and finally yields for the density of states (in the one band case) the expression

$$\rho(\omega) = \sum_{\mathbf{k}} \left( |u_{\mathbf{k}}|^2 \delta(\omega - E_{\mathbf{k}}) + |v_{\mathbf{k}}|^2 \delta(\omega + E_{\mathbf{k}}) \right), \quad (49)$$

which weights the positive and negative eigenvalues according to the composition of the quasiparticle states in terms of the original electrons and holes. For a superconductor with a constant order parameter  $\Delta_0$ , there are no states at  $\omega < \Delta_0$ , and a singularity  $\propto |\omega|/\sqrt{\omega^2 - \Delta_0^2}$  above that energy. For momentum-dependent order parameters, there are no states below the minimum of the order parameter  $\Delta_- = \min_{\mathbf{k}_F} \Delta_{\mathbf{k}_F}$  (at the Fermi surface). Because of the form of the quasiparticle energies  $E_{\mathbf{k}} = \sqrt{\varepsilon_{\mathbf{k}}^2 + |\Delta_{\mathbf{k}}^{s/t}|^2}$ , there appear van Hove singularities in the density of states whenever the order parameter has a minimum or maximum. We note that these singularities arise from minima ( $\Delta_-$ ) or saddle points (at  $\Delta_+ = \max_{\mathbf{k}_F} \Delta_{\mathbf{k}_F}$ ) of the quasiparticle dispersion  $E_{\mathbf{k}}$ . In two dimensions, these lead to steps at  $\omega = \Delta_-$  or logarithmically diverging density of states at the respective energies  $\omega = \Delta_+$  (where also local maxima contribute).

For nodal superconductors, the low-energy density of states is given by the low energy expansion of  $E_{\mathbf{k}}$ . If the order parameter exhibits a (simple) sign-change this leads to a linear quasiparticle dispersion (Dirac-cone) close the node and therefore in the simplest case to a linear density of states close to  $\omega = 0$ . This behavior is identical for nodes dictated by symmetry (for example  $d$ -wave order parameter) as well as accidental nodes (for example  $s_{\pm}$  order parameter). Low temperature expansions of thermodynamic properties such as specific heat, penetration depth (superfluid density) and thermal transport can be calculated from the low energy expansion of the density of states. Thus, these quantities have imprints of the order parameter, and corresponding power law dependencies in the experimental data are used to examine the superconducting order parameter.

The electronic density of states itself can be measured in (scanning) tunneling experiments where the differential conductance is to a good approximation given by  $dI/dV \propto \rho(\omega)$  [41], while there might be corrections from tunneling processes through the surface layers [42, 43]. Some examples of densities of states for unconventional superconducting states in single and multiband systems are shown in Fig. 15 where it becomes obvious that the symmetry of the

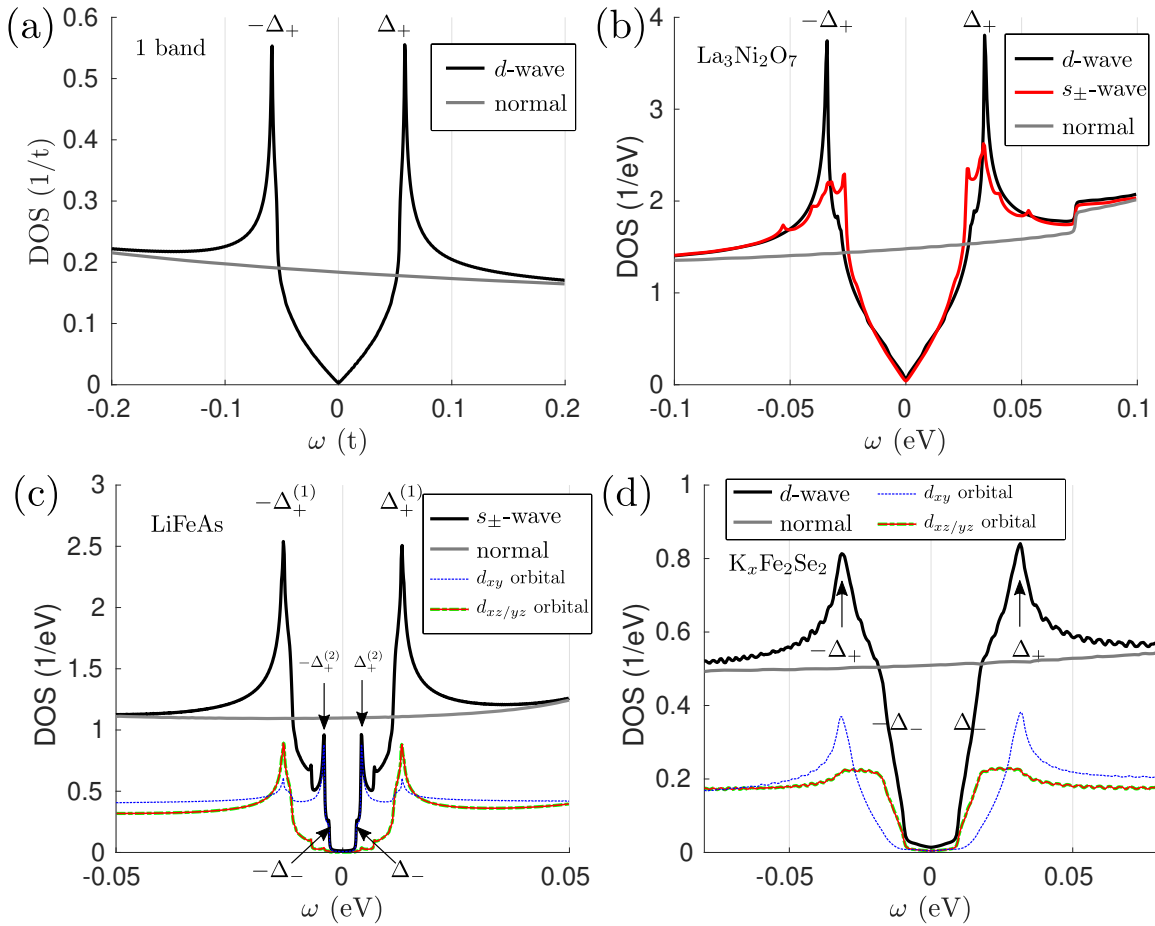


**Fig. 15:** Examples of densities of states for unconventional superconductors: (a) single band model with  $d$ -wave order parameter (see Fig. 8, panel (3) left) exhibiting logarithmically divergent coherence peaks and a linear DOS as low energies from the Dirac-like dispersion close to the nodal points (in two dimensions). (b) Multiband result for bilayer nickelate system where the leading  $d$ -wave instability (see Fig. 12(a)) shows the characteristic behavior known from the single band case, but also a sub-leading  $s_{\pm}$  state has almost identical spectral signatures. (c) DOS for sign changing  $s_{\pm}$  state without nodes. Multiple coherence peaks for gap maxima on the pockets (see Fig. 12(b)) appear. (d) The nodeless  $d$ -wave solution for the system with only electronlike pockets shows coherence peaks and a step at the minimum of the order parameter on the Fermi surface, compare Fig. 12(c).

order parameter cannot always be deduced from the spectrum. There are cases where sign-changing  $s$ -wave and  $d$ -wave states are almost identical (panel b) for the nodal case. Also the fully gapped situation can occur from different symmetries of the order parameter (panels c,d).

## 4.2 Bound states from impurities

The effect of disorder can be used to distinguish conventional from unconventional superconductors and eventually also differentiate between different symmetries of unconventional superconductivity. Here, we will concentrate on the effect of a single impurity in a superconductor [44].

In order to investigate the response of the Cooper pair wavefunction of different pairing candidates to single impurities, we introduce a nonmagnetic impurity or a (classical) magnetic impurity as a variation of the onsite potential via the matrix

$$\widehat{H}_{\text{imp}} = V\tau^z \otimes M \quad (50)$$

for a potential scatterer, and

$$\widehat{H}_{\text{imp}} = S_z\tau^0 \otimes M \quad (51)$$

for a magnetic impurity, where the matrix  $M$  contains the structure of the impurity in the auxiliary quantum numbers, i.e.,  $M = 1$  for a single band model. The basis is again as for Eq. (44). The effect of disorder on the superconducting order parameter itself will be neglected in this section; on the mean-field level one can however treat it self-consistently by solving the BCS equation, Eq. (4), in real space. For some physical observables (especially if states from multiple impurities overlap), this might be important. However for the presence and properties of bound states on single impurities as discussed here, there is no qualitative difference. Assuming no effect on the order parameter itself as mentioned above, the full Green function in real space can be calculated within the  $T$ -matrix approximation as

$$\widehat{G}(\mathbf{r}, \mathbf{r}', \omega) = \widehat{G}^{(0)}(\mathbf{r}-\mathbf{r}', \omega) + \widehat{G}^{(0)}(\mathbf{r}, \omega) \widehat{T}(\omega) \widehat{G}^{(0)}(-\mathbf{r}', \omega), \quad (52)$$

with the  $T$ -matrix given by

$$\widehat{T}(\omega) \equiv \left( \mathbb{1} - \widehat{H}_{\text{imp}} \widehat{G}^{(0)}(\mathbf{0}, \omega) \right)^{-1} \widehat{H}_{\text{imp}}. \quad (53)$$

Here, the free real-space Green function is calculated by the Fourier transform from Eq. (45),

$$\widehat{G}^{(0)}(\mathbf{r}, \omega) = \frac{1}{N} \sum_{\mathbf{k}} \widehat{G}^{(0)}(\mathbf{k}, \omega) e^{i\mathbf{k}\cdot\mathbf{r}}. \quad (54)$$

Having the real space Green function at hand, we can calculate the spin-summed electronic local density of states (LDOS) at auxiliary quantum number  $\alpha$

$$\rho_{\alpha}(\mathbf{r}, \omega) = -\frac{1}{\pi} \text{Im} \left( G_{\alpha\alpha}(\mathbf{r}, \mathbf{r}, \omega) + G_{\bar{\alpha}\bar{\alpha}}(\mathbf{r}, \mathbf{r}, -\omega) \right). \quad (55)$$

**Conventional and unconventional single band superconductors** For the single band case in a conventional superconductor ( $\Delta_{\mathbf{k}} = \Delta$ ), the calculation of the effect of a single (non)magnetic impurity can be done analytically. Using Eq. (46), we can calculate the local Green functions with the result for the diagonal part

$$G_{11}^{(0)}(\omega) = -\frac{\pi\rho(0)\omega}{\sqrt{|\Delta|^2 - \omega^2}} \quad (56)$$

and the off-diagonal part

$$G_{1\bar{1}}^{(0)}(\omega) = \frac{\pi\rho(0)\Delta}{\sqrt{|\Delta|^2 - \omega^2}}. \quad (57)$$

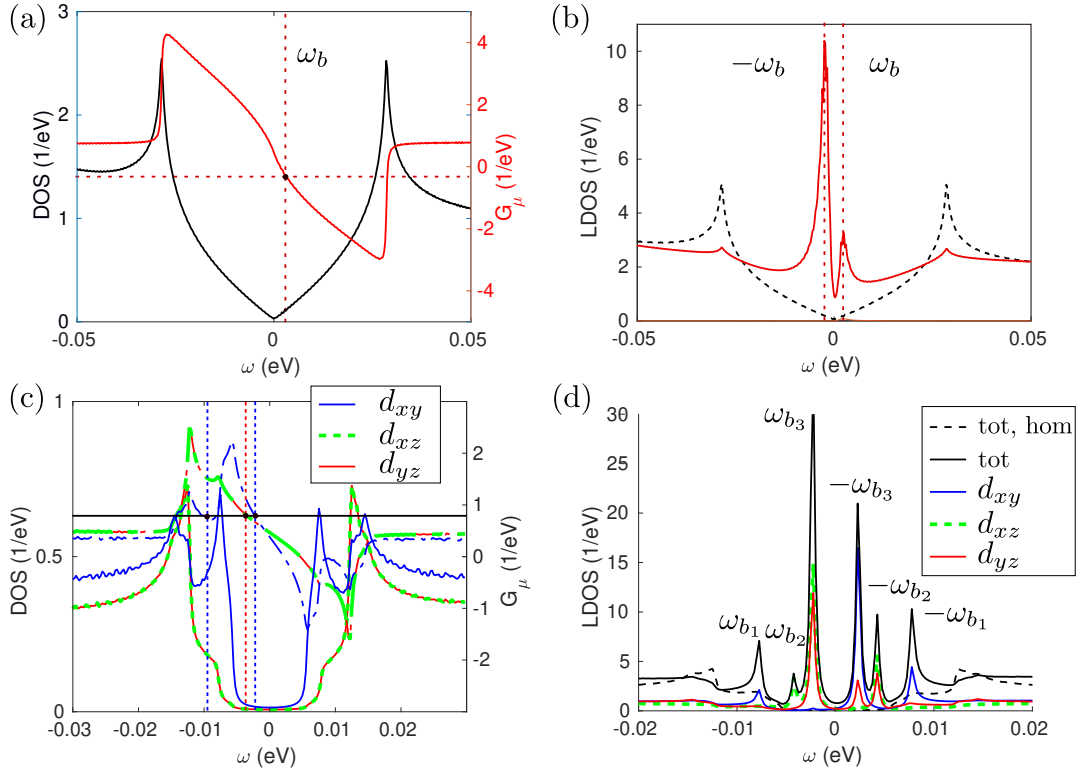


**Fig. 16:** Impurity bound states in unconventional superconductors (a) In a  $d$ -wave superconductor, the real part of the local green function matches the inverse of the impurity potential (black dot),  $1/V = \text{Re} G_{11}(\omega_b)$ . At the bound state energy, the density of states is nonzero, but small. The different weights of the peaks are due to the properties of the free Green function in Eq. (52). (b) Corresponding LDOS exhibiting two impurity peaks from  $\pm\omega_b$  with small broadening. (c) For a multiband system, the analysis is a bit more complicated, but matching  $1/V = \text{Re} G_{11}^\mu(\omega_{b_i})$  for each orbital component yields the correct number of impurity resonances that occur in the LDOS (d). Note that the weight in the individual orbitals is again due to the free Green function  $\hat{G}^{(0)}(\mathbf{r}-\mathbf{r}', \omega)$ , here with  $\mathbf{r} = [1, 0]$ , i.e., spectra next to the impurity.

Finding solutions for  $\omega$  where the  $T$ -matrix diverges is only possible for a magnetic impurity, but not for a non-magnetic impurity in this case. This is just the finding that there are bound states within the gap [45–47] for magnetic impurities, while non-magnetic potentials do not lead to those (Anderson’s theorem) [48]. For a  $d$ -wave superconductor (and other order parameters that average to zero over the Brillouin zone)  $\sum_{\mathbf{k}} \Delta_{\mathbf{k}} = 0$ , also the anomalous Green function vanishes,  $G_{11}^{(0)}(\omega) = 0$ , such that bound state solutions exist for magnetic and nonmagnetic impurities. Since the density of states for nodal superconductors is finite, these bound states have a finite lifetime [44]. Examples of impurity bound states are shown in Fig. 16 for a single band  $d$ -wave superconductor and the multiband system LiFeAs which exhibits multiple bound states for each orbital channel that can become sharp because of the vanishing DOS at low energies of this fully gapped superconductor (compare Fig. 15(c)).

Introducing non-magnetic disorder into superconductors and the measurements of the LDOS close to these impurities can be used to identify unconventional superconductors: If there is a bound state, the superconductor has to be unconventional. The opposite conclusion is however not true in general as it is discussed in the following for the kagome lattice.

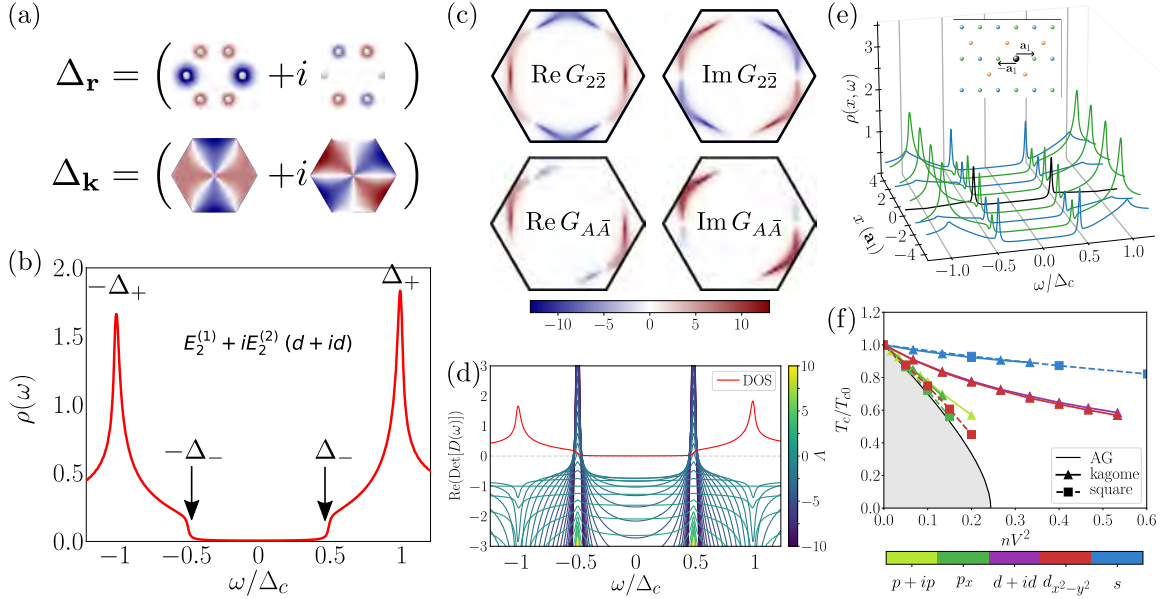


**Fig. 17:** Absence of pair breaking in unconventional superconductors on the kagome lattice: (a)  $d+id$  order parameter in real space  $\Delta_{\mathbf{r}}$  with onsite pairing on the three sublattices and in momentum space ( $\Delta_{\mathbf{k}}$ ) with characteristic sign-changing structure. (b) Density of states yielding a fully gapped system. (c) The Green function in band space  $G_{2\bar{2}}$  averages to zero as in usual  $d$ -wave superconductors, but the sublattice interference makes the Green function in sublattice space  $G_{A\bar{A}}$  not to vanish and protects superconductivity from pairbreaking. (d) No resonances in the  $T$ -matrix within the fully gapped energy such that (e) no impurity bound states from potential scatterers exist. (f) Also  $T_c$  is protected from a fast suppression in  $d$  wave superconductors on the kagome lattice (triangles) [49].

**The case of the kagome lattice** As discussed above, the kagome lattice exhibits three sublattices and generically, single pointlike impurities are located either on the  $A$ ,  $B$ , or  $C$  sublattice. To be concrete, we assume a single nonmagnetic impurity on the  $A$  sublattice. Following the outline above, the  $T$ -matrix calculation can be used with the choice  $M_{ij} = \delta_{1i}\delta_{1j}$  in Eq. (50). Choosing an order parameter of the type  $d+id$  which might be a candidate order parameter because of (i) indications of time reversal symmetry breaking in the superconducting state [40] and (ii) suggestions of this order parameter from spin-fluctuation pairing calculations [30], the  $T$ -matrix calculation is done. The BdG Hamiltonian is set up from the normal state Hamiltonian, Eq. (41), and the order parameter that is onsite in the elementary cell (but exhibits sign change between the sublattices, see Fig. 17(a)) [49]

$$\Delta_{d+id} = \Delta_0 \left( f_{\text{OS}, E_2^{(1)}}^S + i f_{\text{OS}, E_2^{(2)}}^S \right), \quad (58)$$

with the matrices

$$f_{\text{OS}, E_2^{(1)}}^S = \frac{1}{\sqrt{6}} \begin{pmatrix} +1 & 0 & 0 \\ 0 & -2 & 0 \\ 0 & 0 & +1 \end{pmatrix} \quad \text{and} \quad f_{\text{OS}, E_2^{(2)}}^S = \frac{1}{\sqrt{2}} \begin{pmatrix} +1 & 0 & 0 \\ 0 & 0 & 0 \\ 0 & 0 & -1 \end{pmatrix}. \quad (59)$$

While the individual order parameters (in band space) have symmetry-imposed nodes (see Fig. 17(a)), we obtain a fully gapped density of states of the homogeneous system because of

the complex linear combination of the two order parameters. There are steps from the minima of  $|\Delta_{\mathbf{k}}|$  at  $\Delta_-$  in band space and coherence peaks at the maximum gap  $\Delta_+$  (Fig. 17(b)).

Considering single impurity disorder on the sublattice positions, it turns out that the important quantity entering the  $T$ -matrix calculation is the Green function in sublattice space where the momentum dependence is basically a product of the order parameter in band space with the matrix elements (as also evident when looking at the spectral representation of the Green function, Eq. (28)). Unlike the Green function in band space  $G_{2\bar{2}}(\mathbf{k}, \omega)$ , the one in sublattice space  $G_{A\bar{A}}(\mathbf{k}, \omega)$  does not average to zero when calculating the local Green function according to Eq. (54), see (Fig. 17(c)). This means that there is no root of the denominator in Eq. (53) (panel (d)) and no in-gap bound state exists as shown in panel (e) where LDOS spectra at the impurity (black) and along a path to and away from the impurity are shown. From the same physical mechanism  $d$ -wave superconductivity remains robust under presence of pointlike disorder. The suppression of the critical temperature  $T_c$  follows rather the trend for a conventional superconductor than the Abrikosov-Gorkov (AG) [50] law, see Fig. 17 (f) [49].

### 4.3 Dynamical susceptibility and neutron resonance

In section 3, we have discussed the behavior of the (static,  $\omega = 0$ ) susceptibility from a perspective of Fermi surface nesting and deduced the expected superconducting pair states in a spin-fluctuation pairing mechanism. The spin susceptibility can be accessed experimentally in inelastic neutron scattering experiments. This information can be used to either verify whether the theoretical framework for obtaining the spin susceptibility works for the material under consideration, or in a more bottom up approach, one can directly use the measured spin susceptibility as input for calculations of the superconducting pairing.

Once it is established that there are strong spin fluctuations in a superconductive material, more can be learned from the change of the spin fluctuations in the superconducting state. The first observation is a reduction of the spin-response at energies  $\omega \leq 2\Delta_-$  ( $\omega \leq 2\Delta_0$ ) because for gapped superconductors, there are no quasiparticles (less quasiparticles) within this energy range. Second, for unconventional superconductors (with sign change), an enhancement of the spin-fluctuations for momenta  $\mathbf{q}$  connecting parts of the Fermi surface with opposite sign,  $\Delta_{\mathbf{k}} = -\Delta_{\mathbf{k}+\mathbf{q}}$ , is achieved; the so-called neutron resonance as observed in cuprate materials and Fe-based systems. From the energy of the resonance obtained by subtracting intensities above  $T_c$  from the intensities measured below  $T_c$ , one can draw conclusions about the  $\Delta/T_c$  ratio and connect the superconducting material to the weak or strong coupling regime.

The starting point of the calculation of the susceptibility in the superconducting state is Eq. (15), but now, we need to take into account the anomalous Green functions as well, i.e., obtain

$$\begin{aligned} \chi_0^{+-}(\mathbf{q}, \tau) &= -\frac{1}{N} \sum_{\mathbf{k}, \mathbf{k}'} \left( \langle T_\tau c_{\mathbf{k}', \uparrow}(0) c_{\mathbf{k}+\mathbf{q}, \uparrow}^\dagger(\tau) \rangle \langle T_\tau c_{\mathbf{k}, \downarrow}(\tau) c_{\mathbf{k}'-\mathbf{q}, \downarrow}^\dagger(0) \rangle \right. \\ &\quad \left. + \langle T_\tau c_{\mathbf{k}'-\mathbf{q}, \downarrow}^\dagger(0) c_{\mathbf{k}+\mathbf{q}, \uparrow}^\dagger(\tau) \rangle \langle T_\tau c_{\mathbf{k}, \downarrow}(\tau) c_{\mathbf{k}', \uparrow}(0) \rangle \right) \\ &= -\frac{1}{N} \sum_{\mathbf{k}} \left( G_{11}^0(\mathbf{k}+\mathbf{q}, -\tau) G_{1\bar{1}}^0(\mathbf{k}, \tau) + G_{1\bar{1}}^0(\mathbf{k}+\mathbf{q}, -\tau) G_{11}^0(\mathbf{k}, \tau) \right), \quad (60) \end{aligned}$$

where we used a similar notation as in Eq. (45) for the anomalous Green function. Again, for the single band case, we can use the analytical result for the Green function in frequency space, Eq. (46) to obtain a closed expression of the susceptibility

$$\begin{aligned} \chi_0^{+-}(\mathbf{q}, \omega) = \frac{1}{\mathcal{N}} \sum_{\mathbf{k}, E>0} \left[ \left( 1 - \frac{\varepsilon_{\mathbf{k}}\varepsilon_{\mathbf{k}+\mathbf{q}} + \Delta_{\mathbf{k}+\mathbf{q}}^*\Delta_{\mathbf{k}}}{E_{\mathbf{k}}E_{\mathbf{k}+\mathbf{q}}} \right) \frac{1 - f(E_{\mathbf{k}}) - f(E_{\mathbf{k}+\mathbf{q}})}{\omega + E_{\mathbf{k}+\mathbf{q}} + E_{\mathbf{k}} + i\eta} \right. \\ + \left( 1 - \frac{\varepsilon_{\mathbf{k}}\varepsilon_{\mathbf{k}+\mathbf{q}} + \Delta_{\mathbf{k}+\mathbf{q}}^*\Delta_{\mathbf{k}}}{E_{\mathbf{k}}E_{\mathbf{k}+\mathbf{q}}} \right) \frac{f(E_{\mathbf{k}}) + f(E_{\mathbf{k}+\mathbf{q}}) - 1}{\omega - E_{\mathbf{k}+\mathbf{q}} - E_{\mathbf{k}} + i\eta} \\ + \left( 1 + \frac{\varepsilon_{\mathbf{k}}\varepsilon_{\mathbf{k}+\mathbf{q}} + \Delta_{\mathbf{k}+\mathbf{q}}^*\Delta_{\mathbf{k}}}{E_{\mathbf{k}}E_{\mathbf{k}+\mathbf{q}}} \right) \frac{f(E_{\mathbf{k}}) - f(E_{\mathbf{k}+\mathbf{q}})}{\omega + E_{\mathbf{k}+\mathbf{q}} - E_{\mathbf{k}} + i\eta} \\ \left. + \left( 1 + \frac{\varepsilon_{\mathbf{k}}\varepsilon_{\mathbf{k}+\mathbf{q}} + \Delta_{\mathbf{k}+\mathbf{q}}^*\Delta_{\mathbf{k}}}{E_{\mathbf{k}}E_{\mathbf{k}+\mathbf{q}}} \right) \frac{f(E_{\mathbf{k}+\mathbf{q}}) - f(E_{\mathbf{k}})}{\omega + E_{\mathbf{k}} - E_{\mathbf{k}+\mathbf{q}} + i\eta} \right], \quad (61) \end{aligned}$$

where we have performed the Matsubara summation analytically, done the analytical continuation  $i\nu_n \rightarrow \omega + i\eta$  and used the particle-hole symmetry of the BdG Hamiltonian to rewrite the summation in terms of positive energies only. The Hubbard interactions can be taken into account in an RPA approach similar to Eq. (30). Resonances are now divergences in the imaginary part of the susceptibility at the respective frequency  $\omega_0$ . Splitting the susceptibility in real and imaginary part,  $\chi^{+-}(\mathbf{q}, \omega) = \chi^{+-'} + i\chi^{+-''}$ , we can calculate the imaginary part of the susceptibility as follows (dropping the arguments and the transverse label  $+ -$ ),

$$\chi^{+-''} = \text{Im} \frac{\chi^{+-'} + i\chi^{+-''}}{1 - U(\chi^{+-'} + i\chi^{+-''})} = \text{Im} \frac{\chi_0}{1 - U\chi_0} = \frac{\chi_0''}{(1 - U\chi_0')^2 + (U\chi_0'')^2}. \quad (62)$$

This diverges if the numerator vanishes which requires  $1 - U\chi_0' = 0$  (similar as the criterion for the magnetic instability) and  $\chi_0'' \rightarrow 0$  (gapped spectrum). The second is exactly fulfilled for a full gap superconductor because of missing excitations at this energy, the first can be fulfilled in the superconducting state if there is a sign-change in the order parameter as we discuss in the following. The first observation is that the first two terms in Eq. (61) vanish in the normal state when  $\varepsilon_{\mathbf{k}} = E_{\mathbf{k}}$  and  $\Delta_{\mathbf{k}} = 0$ . For states close to the Fermi level, where there is an effect from the superconducting state, we can set  $\varepsilon_{\mathbf{k}} \approx 0$  and obtain  $E_{\mathbf{k}} = |\Delta_{\mathbf{k}}|$  because of the sqrt in the quasiparticle dispersion, Eq. (9). Looking at the coherence factor,

$$\left( 1 - \frac{\Delta_{\mathbf{k}+\mathbf{q}}\Delta_{\mathbf{k}}}{|\Delta_{\mathbf{k}}||\Delta_{\mathbf{k}+\mathbf{q}}|} \right) \approx \begin{cases} 0 \\ 2 \end{cases} \quad (63)$$

it exhibits two values depending on the order parameter: For momenta  $\mathbf{k}$  and  $\mathbf{k}+\mathbf{q}$  with the same sign of the order parameter it vanishes, and for momenta with  $\text{sign } \Delta_{\mathbf{k}+\mathbf{q}}^* = -\text{sign } \Delta_{\mathbf{k}}$  it reaches the value 2. Sign-changing order parameters therefore increase the real susceptibility and lead to the mentioned spin-resonance (when taking into account interactions at least within RPA), while conventional superconductivity (without sign-change) yields just a suppressed susceptibility. Some examples of theoretical investigations in multiband settings on this topic can be found in Refs. [51, 27].

#### 4.4 Spin relaxation rate and Hebel-Slichter peak

As a second example of a spectroscopic probe related to the spin susceptibility, we want to discuss the spin relaxation rate in nuclear magnetoresonance (NMR) experiments. In a typical NMR experiment, the nuclear spins are polarized by an external field and then tilted from the equilibrium position by a radio frequency pulse. Left in this state, the spins precess around the external field and eventually relax to the polarized state because of scattering events from the (conduction) electrons in the system with a relaxation time  $T_1$ . Solving the Bloch equations for the dynamics of the magnetization in presence of electron spins and the hyperfine coupling, leads to the following relation for the longitudinal relaxation due to spin fluctuations [13]

$$\alpha \equiv \frac{1}{T_1 T} \propto \lim_{\omega \rightarrow 0} \frac{1}{\mathcal{N}} \sum_{\mathbf{q}} \text{Im} \frac{\chi_0^{+-}(\mathbf{q}, \omega)}{\omega}. \quad (64)$$

The relevant energy scale is the Larmor frequency  $\omega_L$  that is practically very small,  $\hbar\omega_L \approx 10^{-7}$  eV, so it is considered as the smallest energy scale in the problem, which is the meaning of the limit  $\omega \rightarrow 0$  in the equation above.

The spin susceptibility can now be calculated using Eq. (61) where it turns out that now, the first two terms do not contribute because the energy of the quasiparticles are (almost) always much larger than the very small  $\omega$  in the denominator, so these terms do not contribute to the imaginary part of the susceptibility at low frequencies. Different for the last two terms with the opposite sign of  $E_{\mathbf{k}}$  and  $E_{\mathbf{k}+\mathbf{q}}$  which gives a contribution even in the limit  $\omega \rightarrow 0$ . Close to  $T_c$  where the order parameter is very small, there is an enhancement of the density of states (coherence peak) close to zero energy. This leads to an increase of the integrated spin susceptibility (compared to the normal state) just below  $T_c$ . For a superconductor with a constant gap, the density of states diverges as  $1/\sqrt{\omega^2 - \Delta_0(T)^2}$  while for an anisotropic superconductor with a maximum gap  $\Delta_+$ , there is only a weaker divergence such that there is still a weak enhancement. In this case, the relevant prefactor behaves as

$$\left(1 + \frac{\Delta_{\mathbf{k}+\mathbf{q}}\Delta_{\mathbf{k}}}{|\Delta_{\mathbf{k}}||\Delta_{\mathbf{k}+\mathbf{q}}|}\right) \approx \begin{cases} 2 & \text{same sign} \\ 0 & \text{different sign} \end{cases} \quad (65)$$

at low  $\omega$ . To understand this in more detail, it is instructive to examine the factor

$$B(\mathbf{q}, \mathbf{k}_n) = \frac{\Delta_{\mathbf{k}_n+\mathbf{q}}^* \Delta_{\mathbf{k}_n}}{E_{\mathbf{k}_n} E_{\mathbf{k}_n+\mathbf{q}}}, \quad (66)$$

which for a conventional superconductor (without sign-change) remains finite while for a  $d$ -wave order parameter it averages to zero when integrated over  $\mathbf{k}$  for a fixed  $\mathbf{q}$  as illustrated in Fig. 18(a). This leads to an additional enhancement of the spin relaxation rate  $\alpha$  below  $T_c$  for an  $s$ -wave order parameter while for a sign-changing order parameter only the enhancement from the (weak) peak in the density of states contributes. Experimentally, the absence of a (visible) Hebel-Slichter peak is interpreted as an indication of unconventional superconductivity, while its presence is an indication for a non-sign changing order parameter. See however Ref. [52] for more subtle behavior in unconventional superconductors close to  $T_c$ .

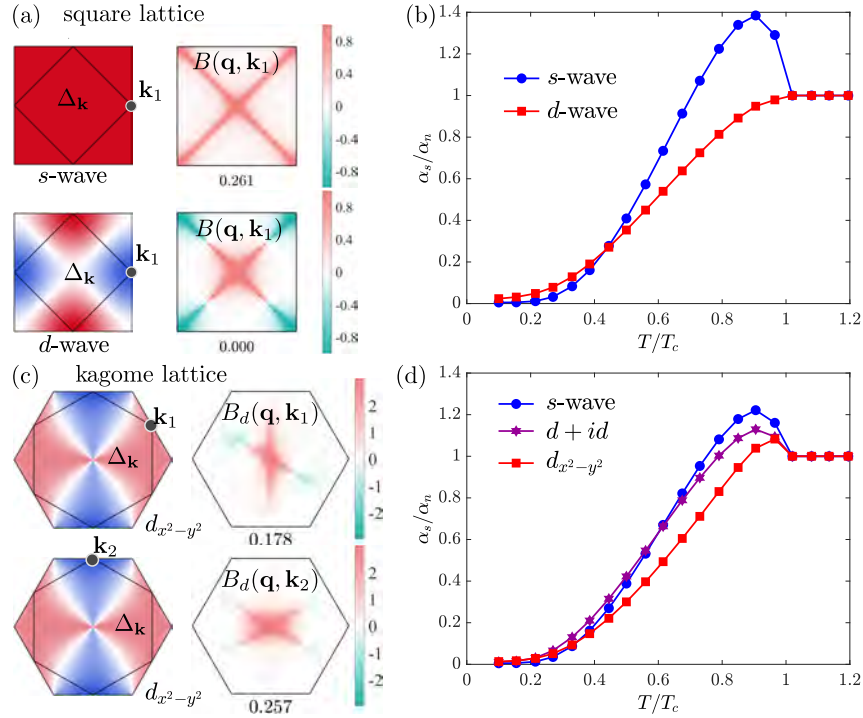


**Fig. 18:** Hebel-Slichter peak for different lattices (a) In the square lattice, the constant order parameter yields a (positive) value of  $B(\mathbf{q}, \mathbf{k}_n)$  everywhere in the Brillouin zone (and independent of the choice of  $\mathbf{k}_n$ ). Yielding a positive integral (0.261 in this case), enhances the spin relaxation rate compared to its normal state value (b). For the d-wave order parameter (lower panels in (a)), the factor  $B(\mathbf{q}, \mathbf{k}_n)$  is always equally positive and negative, such that the integral over it vanishes and no Hebel-Slichter peak is visible. (c) For the kagome lattice, there are positive and negative regions of  $B_d(\mathbf{q}, \mathbf{k}_n)$ , however the negative regions are suppressed because of the different sublattice weight for  $\mathbf{k}$  points far away from  $\mathbf{k}_n$ . In summary, the integral does not average to zero and a Hebel-Slichter peak is expected for unconventional (sign-changing) order parameters as well (d) [53].

We will now discuss that this conclusion does not generally apply for kagome systems, again the peculiar property of the sublattice weight, Fig. 19 plays an important role. Indeed, one can evaluate the multiband generalization of the susceptibility numerically by employing the  $d+id$  superconducting order parameter as already discussed in the previous section, the result is shown in Fig. 18. To gain further insights, we here map the problem to an effective single band Hamiltonian. As seen, in Fig. 19(c), only band number 2 crosses the Fermi level. In the weak coupling regime where the order parameter is much smaller than any band energy scale, only the eigenenergies of this band significantly contribute to Eq. (61) for  $\omega \rightarrow 0$ . To understand the effect on the spin relaxation rate in more detail, we start from the BdG Hamiltonian, Eq. (44) which we transform to the band basis by application of the unitary transformation that diagonalizes  $H_0$ . Then the order parameter from sublattice space to band space transforms as

$$\Delta_{nm}(\mathbf{k}) = u_{n\alpha}^*(\mathbf{k}) \Delta_{\alpha\beta} u_{m\beta}^*(-\mathbf{k}), \quad (67)$$

where  $u_{n\alpha}(\mathbf{k})$  is the eigenstate of  $H_0(\mathbf{k})$  in band  $n$ . For band 2, the effective Hamiltonian now

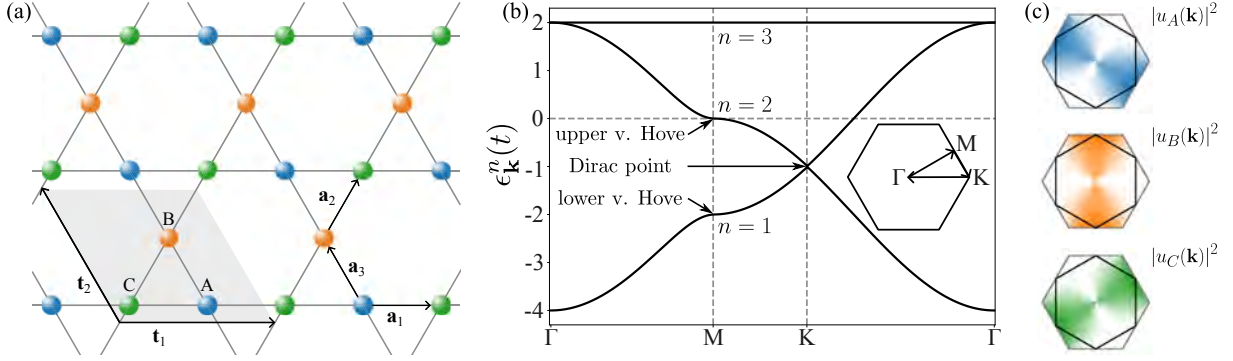


**Fig. 19:** Band structure of simple kagome lattice (a) lattice structure with the three sublattices, the lattice vectors  $\mathbf{t}_i$  and the nearest neighbor vectors  $\mathbf{a}_i$ . (b) Band structure exhibiting van Hove points and a Dirac point. (c) Orbital weight distribution for the  $n = 2$  band that is crossing the Fermi level close to the upper van Hove point.

reads

$$H_{\text{eff}}(\mathbf{k}) = \begin{pmatrix} \varepsilon_{2,\mathbf{k}} & -\Delta_{22}(\mathbf{k}) \\ -\Delta_{22}^*(\mathbf{k}) & -\varepsilon_{2,\mathbf{k}} \end{pmatrix}. \quad (68)$$

Evaluating the susceptibility from this effective Hamiltonian, we see that it acquires an additional factor arising from the transformation from sublattice to band space

$$g_{\alpha\beta}(\mathbf{k}, \mathbf{q}) = u_{2\alpha}(\mathbf{k}+\mathbf{q})u_{2\beta}(\mathbf{k}+\mathbf{q})u_{2\alpha}(\mathbf{k})u_{2\beta}(\mathbf{k}). \quad (69)$$

and the dynamical susceptibility in the superconducting state reads

$$\begin{aligned} \chi_0^{+-}(\mathbf{q}, \omega) = \frac{1}{\mathcal{N}} \sum_{\mathbf{k}, E>0} & \left[ \left( 1 - \frac{\varepsilon_{\mathbf{k}}\varepsilon_{\mathbf{k}+\mathbf{q}} + \Delta_{\mathbf{k}+\mathbf{q}}^*\Delta_{\mathbf{k}}}{E_{\mathbf{k}}E_{\mathbf{k}+\mathbf{q}}} \right) \frac{1 - f(E_{\mathbf{k}}) - f(E_{\mathbf{k}+\mathbf{q}})}{\omega + E_{\mathbf{k}+\mathbf{q}} + E_{\mathbf{k}} + i\eta} \right. \\ & + \left( 1 - \frac{\varepsilon_{\mathbf{k}}\varepsilon_{\mathbf{k}+\mathbf{q}} + \Delta_{\mathbf{k}+\mathbf{q}}^*\Delta_{\mathbf{k}}}{E_{\mathbf{k}}E_{\mathbf{k}+\mathbf{q}}} \right) \frac{f(E_{\mathbf{k}}) + f(E_{\mathbf{k}+\mathbf{q}}) - 1}{\omega - E_{\mathbf{k}+\mathbf{q}} - E_{\mathbf{k}} + i\eta} \\ & + \left( 1 + \frac{\varepsilon_{\mathbf{k}}\varepsilon_{\mathbf{k}+\mathbf{q}} + \Delta_{\mathbf{k}+\mathbf{q}}^*\Delta_{\mathbf{k}}}{E_{\mathbf{k}}E_{\mathbf{k}+\mathbf{q}}} \right) \frac{f(E_{\mathbf{k}}) - f(E_{\mathbf{k}+\mathbf{q}})}{\omega + E_{\mathbf{k}+\mathbf{q}} - E_{\mathbf{k}} + i\eta} \\ & \left. + \left( 1 + \frac{\varepsilon_{\mathbf{k}}\varepsilon_{\mathbf{k}+\mathbf{q}} + \Delta_{\mathbf{k}+\mathbf{q}}^*\Delta_{\mathbf{k}}}{E_{\mathbf{k}}E_{\mathbf{k}+\mathbf{q}}} \right) \frac{f(E_{\mathbf{k}+\mathbf{q}}) - f(E_{\mathbf{k}})}{\omega + E_{\mathbf{k}} - E_{\mathbf{k}+\mathbf{q}} + i\eta} \right] \sum_{\alpha\beta} g_{\alpha\beta}(\mathbf{k}, \mathbf{q}). \end{aligned} \quad (70)$$

In this equation, we have dropped the subscript for the band, i.e.,  $\varepsilon_{2,\mathbf{k}} \rightarrow \varepsilon_{\mathbf{k}}$ ,  $\Delta_{22}(\mathbf{k}) \rightarrow \Delta_{\mathbf{k}}$ . Similarly to the previous discussion, we can define a (dressed) spin-susceptibility coherence factor given by

$$B_d(\mathbf{q}, \mathbf{k}_n) = \frac{\sum_{\alpha\beta} g_{\alpha\beta}(\mathbf{k}_n, \mathbf{q}) \Delta_{\mathbf{k}_n+\mathbf{q}}^* \Delta_{\mathbf{k}_n}}{Z E_{\mathbf{k}_n} E_{\mathbf{k}_n+\mathbf{q}}}, \quad (71)$$

where  $Z$  is a normalization factor defined by  $Z = \frac{1}{\mathcal{N}^2} \sum_{\mathbf{k}, \mathbf{q}} \sum_{\alpha\beta} g_{\alpha\beta}(\mathbf{k}, \mathbf{q})$ . The crucial property of Eq. (71) is now that it contains a product of the order parameter (in band space) which

has sign changing and compensation properties for a  $d$ -wave order parameter, but is additionally multiplied by the sublattice weights that vanish in parts of the Brillouin zone, especially where the order parameter has opposite sign. Consequently, the averaging is only partial and an unconventional  $d$  (or  $d+id$ ) order parameter acquires a finite enhancement factor leading to a sizeable Hebel-Slichter peak just below  $T_c$ . In other words for the kagome lattice, one expects Hebel-Slichter peaks for conventional and unconventional order parameters (Fig. 18(d)) and its presence should not be interpreted as evidence against unconventional pairing in these systems [53].

## Acknowledgements

I thank Morten Holm Christensen for discussions about the structure of these lecture notes. Thanks to Brian Møller Andersen and Mercè Roig for proofreading and useful comments and to Yi Dai and Sofie Castro Holbæk for the collaboration on the topics of kagome superconductors.

## References

- [1] F. Steglich, J. Aarts, C.D. Bredl, W. Lieke, D. Meschede, W. Franz, and H. Schäfer, *Phys. Rev. Lett.* **43**, 1892 (1979)
- [2] D. Jérôme, A. Mazaud, M. Ribault, and K. Bechgaard, *J. Phys. Lett.* **41**, 95 (1980)
- [3] J.G. Bednorz and K.A. Müller, *Z. Phys. B* **64**, 189 (1986)
- [4] A.F. Hebard, M.J. Rosseinsky, R.C. Haddon, D.W. Murphy, S.H. Glarum, T.T.M. Palstra, A.P. Ramirez, and A.R. Kortan, *Nature* **350**, 600 (1991)
- [5] Y. Maeno, H. Hashimoto, K. Yoshida, S. Nishizaki, T. Fujita, J.G. Bednorz, and F. Lichtenberg, *Nature* **372**, 532 (1994)
- [6] Y. Kamihara, H. Hiramatsu, M. Hirano, R. Kawamura, H. Yanagi, T. Kamiya, and H. Hosono, *J. Am Chem. Soc.* **128**, 10012 (2006)
- [7] J. Nagamatsu, N. Nakagawa, T. Muranaka, Y. Zenitani, and J. Akimitsu, *Nature* **410**, 63 (2001)
- [8] A.P. Drozdov, M.I. Eremets, I.A. Troyan, V. Ksenofontov, and S.I. Shylin, *Nature* **525**, 73 (2015)
- [9] B.R. Ortiz, S.M.L. Teicher, Y. Hu, J.L. Zuo, P.M. Sarte, E.C. Schueller, A.M.M. Abeykoon, M.J. Krogstad, S. Rosenkranz, R. Osborn, R. Seshadri, L. Balents, J. He, and S.D. Wilson, *Phys. Rev. Lett.* **125**, 247002 (2020)
- [10] D.J. Scalapino, *Rev. Mod. Phys.* **84**, 1383 (2012)
- [11] F. Lechermann, *Phys. Rev. X* **10**, 041002 (2020)
- [12] A. Chubukov and P.J. Hirschfeld, *Phys. Today* **68**, 46 (2015)
- [13] P. Coleman: *Introduction to Many-Body Physics* (Cambridge University Press, 2015)
- [14] P.J. Hirschfeld, M.M. Korshunov, and I.I. Mazin, *Rep. Prog. Phys.* **74**, 124508 (2011)
- [15] M. Sigrist and K. Ueda, *Rev. Mod. Phys.* **63**, 239 (1991)
- [16] S. Panda and P.J. Hirschfeld, *Phys. Rev. B* **109**, 174504 (2024)
- [17] H. Bruus and K. Flensberg, *Many-body quantum theory in condensed matter physics* (Oxford University Press, 2004)
- [18] W. Kohn and J.M. Luttinger, *Phys. Rev. Lett.* **15**, 524 (1965)
- [19] A. Kreisel, Y. Quan, and P.J. Hirschfeld, *Phys. Rev. B* **105**, 104507 (2022)

- [20] A.T. Rømer, T.A. Maier, A. Kreisel, I. Eremin, P.J. Hirschfeld, and B.M. Andersen, *Phys. Rev. Res.* **2**, 013108 (2020)
- [21] A. Kreisel, A.T. Rømer, P.J. Hirschfeld, and B.M. Andersen, *J. Supercond. Nov. Magn.* **30**, 85 (2017)
- [22] S. Graser, T.A. Maier, P.J. Hirschfeld, and D.J. Scalapino, *New J. Phys.* **11**, 025016 (2009)
- [23] Y. Maeno, S. Yonezawa, and A. Ramires, arXiv:2402.12117 (2024)
- [24] M.R. Norman, *Physics* **13**, 85 (2020)
- [25] H. Liu, C. Xia, S. Zhou, and H. Chen, arXiv:2311.07316 (2023)
- [26] A. Kreisel, R. Nelson, T. Berlijn, W. Ku, R. Aluru, S. Chi, H. Zhou, U.R. Singh, P. Wahl, R. Liang, W.N. Hardy, D.A. Bonn, P.J. Hirschfeld, and B.M. Andersen, *Phys. Rev. B* **94**, 224518 (2016)
- [27] T.A. Maier, S. Graser, P.J. Hirschfeld, and D.J. Scalapino, *Phys. Rev. B* **83**, 100515 (2011)
- [28] K. Kuroki, S. Onari, R. Arita, H. Usui, Y. Tanaka, H. Kontani, and H. Aoki, *Phys. Rev. Lett.* **101**, 087004 (2008)
- [29] A.F. Kemper, T.A. Maier, S. Graser, H.-P. Cheng, P.J. Hirschfeld, and D.J. Scalapino, *New J. Phys.* **12**, 073030 (2010)
- [30] A.T. Rømer, S. Bhattacharyya, R. Valentí, M.H. Christensen, and B.M. Andersen, *Phys. Rev. B* **106**, 174514 (2022)
- [31] C.M. Puetter and H.-Y. Kee, *EPL (Europhys. Lett.)* **98**, 27010 (2012)
- [32] M. Roig, A.T. Rømer, A. Kreisel, P.J. Hirschfeld, and B.M. Andersen, *Phys. Rev. B* **106**, L100501 (2022)
- [33] H. Sun, M. Huo, X. Hu, J. Li, Z. Liu, Y. Han, L. Tang, Z. Mao, P. Yang, B. Wang, J. Cheng, D.-X. Yao, G.-M. Zhang, and M. Wang, *Nature* **621**, 493 (2023)
- [34] F. Lechermann, J. Gondolf, S. Bötzel, and I.M. Eremin, *Phys. Rev. B* **108**, L201121 (2023)
- [35] M. Tomić: *Ab-initio simulations of pressure effects on structural and electronic properties of iron based superconductors* (PhD thesis, Univ. Frankfurt, 2015)
- [36] S.K. Ghosh, M. Smidman, T. Shang, J.F. Annett, A.D. Hillier, J. Quintanilla, and H. Yuan, *J. Phys.: Condens. Matter* **33**, 033001 (2020)
- [37] B.M. Andersen, A. Kreisel, and P.J. Hirschfeld, *Front. Phys.* **12**, 1353425 (2024)

- [38] H.S. Røising, M. Geier, A. Kreisel, and B.M. Andersen, *Phys. Rev. B* **109**, 054521 (2024)
- [39] H.-S. Xu, Y.-J. Yan, R. Yin, W. Xia, S. Fang, Z. Chen, Y. Li, W. Yang, Y. Guo, and D.-L. Feng, *Phys. Rev. Lett.* **127**, 187004 (2021)
- [40] C. Mielke, D. Das, J.-X. Yin, H. Liu, R. Gupta, Y.-X. Jiang, M. Medarde, X. Wu, H.C. Lei, J. Chang, P. Dai, Q. Si, H. Miao, R. Thomale, T. Neupert, Y. Shi, R. Khasanov, M.Z. Hasan, H. Luetkens, and Z. Guguchia, *Nature* **602**, 245 (2022)
- [41] J.E. Hoffman, *Rep. Prog. Phys.* **74**, 124513 (2011)
- [42] I. Martin, A.V. Balatsky, and J. Zaanen, *Phys. Rev. Lett.* **88**, 097003 (2002)
- [43] A. Kreisel, P. Choubey, T. Berlijn, W. Ku, B.M. Andersen, and P.J. Hirschfeld, *Phys. Rev. Lett.* **114**, 217002 (2015)
- [44] A.V. Balatsky, I. Vekhter, and J.-X. Zhu, *Rev. Mod. Phys.* **78**, 373 (2006)
- [45] L. Yu, *Acta Phys. Sin.* **21**, 75 (1965)
- [46] H. Shiba, *Prog. Theor. Phys.* **40**, 435 (1968)
- [47] A. Rusinov, *Sov. Phys. JETP* **29**, 1101 (1969)
- [48] P. Anderson, *J. Phys. Chem. Solids* **11**, 26 (1959)
- [49] S.C. Holbæk, M.H. Christensen, A. Kreisel, and B.M. Andersen, *Phys. Rev. B* **108**, 144508 (2023)
- [50] A.A. Abrikosov and L.P. Gor'kov: *Zh. Eksp. Teor. Fiz.* **39**, 1781 (1960)
- [51] T.A. Maier, S. Graser, D.J. Scalapino, and P.J. Hirschfeld, *Phys. Rev. B* **79**, 134520 (2009)
- [52] D. Parker and S. Haas, *Phys. Rev. B* **75**, 052501 (2007)
- [53] Y. Dai, A. Kreisel, and B.M. Andersen, *arXiv:2404.10835* (2024)